RASA1 maintains the lymphatic vasculature in a quiescent functional state in mice

Philip E. Lapinski,[1] Sunkuk Kwon,[2] Beth A. Lubeck,[1] John E. Wilkinson,[3] R. Sathish Srinivasan,[4] Eva Sevick-Muraca,[2] and Philip D. King[1]

[1]Department of Microbiology and Immunology, University of Michigan Medical School, Ann Arbor, Michigan, USA. [2]Center for Molecular Imaging, Brown Foundation Institute for Molecular Medicine, University of Texas Health Science Center, Houston, Texas, USA. [3]Unit for Laboratory Animal Medicine, University of Michigan Medical School, Ann Arbor, Michigan, USA. [4]Department of Genetics and Tumor Cell Biology, St. Jude Children's Hospital, Memphis, Tennessee, USA.

RASA1 (also known as p120 RasGAP) is a Ras GTPase–activating protein that functions as a regulator of blood vessel growth in adult mice and humans. In humans, *RASA1* mutations cause capillary malformation–arteriovenous malformation (CM-AVM); whether it also functions as a regulator of the lymphatic vasculature is unknown. We investigated this issue using mice in which *Rasa1* could be inducibly deleted by administration of tamoxifen. Systemic loss of RASA1 resulted in a lymphatic vessel disorder characterized by extensive lymphatic vessel hyperplasia and leakage and early lethality caused by chylothorax (lymphatic fluid accumulation in the pleural cavity). Lymphatic vessel hyperplasia was a consequence of increased proliferation of lymphatic endothelial cells (LECs) and was also observed in mice in which induced deletion of *Rasa1* was restricted to LECs. RASA1-deficient LECs showed evidence of constitutive activation of Ras in situ. Furthermore, in isolated RASA1-deficient LECs, activation of the Ras signaling pathway was prolonged and cellular proliferation was enhanced after ligand binding to different growth factor receptors, including VEGFR-3. Blockade of VEGFR-3 was sufficient to inhibit the development of lymphatic vessel hyperplasia after loss of RASA1 in vivo. These findings reveal a role for RASA1 as a physiological negative regulator of LEC growth that maintains the lymphatic vasculature in a quiescent functional state through its ability to inhibit Ras signal transduction initiated through LEC-expressed growth factor receptors such as VEGFR-3.

Introduction

Ras is a small inner membrane–tethered GTP-binding protein that regulates cell growth, survival, and differentiation (1). Stimulation of cells with growth factors results in recruitment of guanine nucleotide exchange factors (GEFs) to membranes that switch Ras from an inactive GDP-bound to an active GTP-bound state (2). GEFs eject GDP from the Ras guanine nucleotide–binding pocket, thereby allowing Ras to bind GTP. In its GTP-bound state, Ras triggers the activation of several different downstream signal transduction pathways, including the MAPK pathway, which couples membrane events to cellular responses (3). Appropriate growth factor–induced signal transduction requires subsequent inactivation of Ras through hydrolysis of bound GTP to GDP (2). However, Ras has only weak GTPase activity, and efficient conversion of Ras back to its GDP-bound form requires physical interaction with Ras GTPase–activating proteins (RasGAPs). RasGAPs increase the ability of Ras to hydrolyze GTP by several orders of magnitude (2).

Numerous RasGAPs have now been identified, many of which have overlapping patterns of tissue expression (4). Therefore, which RasGAPs regulate Ras activation in which tissues has yet to be resolved. One of the first described RasGAPs is p120 RasGAP (RASA1). Despite potential redundancy of function with other RasGAPs, mouse gene knockout studies have indicated an important role for this RasGAP in the control of blood vessel development during embryogenesis (5). In mice homozygous for a targeted null allele of *Rasa1*, blood vessel endothelial cells (BECs) fail to organize into a honeycombed network within yolk sacs. In addition, within the embryo, blood vessel growth abnormalities and vessel ruptures are observed, resulting in leakage of blood into the embryo and death at E10.5 (5).

RASA1 also plays an important role as a regulator of blood vessel growth in adult mice. Specifically, recent evidence indicates that RASA1 functions as a negative regulator of blood vessel angiogenesis triggered in response to tumors or purified angiogenic growth factors, such as FGF (6). Furthermore, a microRNA has been identified that has specificity for RASA1 and whose expression is strongly induced in BECs by angiogenic growth factors. Induction of this microRNA in BECs during the course of angiogenesis results in downregulation of RASA1 expression. This event is required for continuation of the angiogenic response (6).

In addition to mice, RASA1 regulates blood vessel growth in humans. Capillary malformation–arteriovenous malformation (CM-AVM; OMIM 608355) is caused by germline mutations of *RASA1* that act in a dominant fashion with high penetrance (7–9). Capillary malformation in this disease results in the appearance of single or multiple pink cutaneous lesions. In addition, in about one-third of patients, there are fast flow lesions, including intracranial arteriovenous malformations, arteriovenous fistulas, and Parkes-Weber Syndrome. Mutations are distributed randomly throughout the *RASA1* gene and include nonsense, missense, and splice-site substitutions as well as insertions and deletions resulting in frame shifts or splice site disruption. In affected individuals, it is hypothesized that disease results from somatic mutation of the normal allele, consistent with the focal nature of lesions.

Concerning the lymphatic vascular system, strict control over Ras signaling would seem paramount. In transgenic mice, overexpression of Ras in endothelial cells results in lymphatic vessel hyperplasia and leakage in the form of tissue edema and chylothorax (10); however, disorders of blood vessel growth and function

Conflict of interest: The authors have declared that no conflict of interest exists.
Citation for this article: *J Clin Invest.* 2012;122(2):733–747. doi:10.1172/JCI46116.

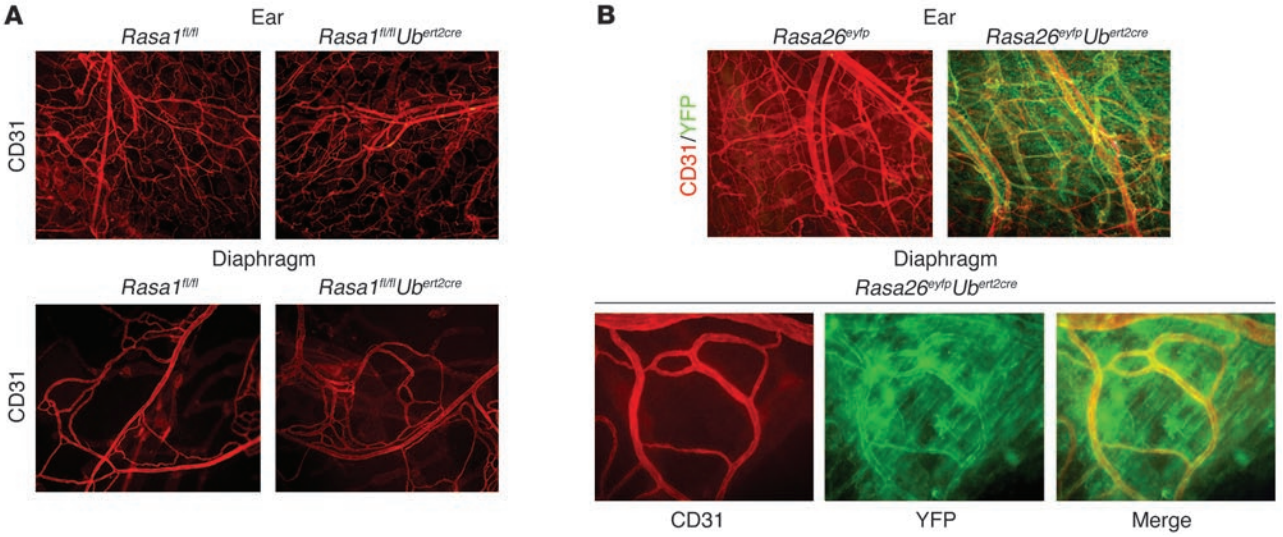

Figure 1
Absence of blood vessel abnormalities in induced RASA1-deficient mice. (**A**) Whole mount staining of ear and diaphragm from *Rasa1*$^{fl/fl}$*Ub*^{ert2cre} transgenic and *Rasa1*$^{fl/fl}$ control mice (treated with TM 4 months prior) for the BEC marker CD31. (**B**) Adult *Rosa26*^{eyfp} and *Rosa26*^{eyfp}*Ub*^{ert2cre} mice were administered TM at 2 months of age and again 10 days later. 7 days after the last TM injection, whole mount ear and thoracic diaphragm specimens were stained with anti-GFP antibodies to identify sites of YFP expression (green) and anti-CD31 antibodies to identify blood vessels (red). Merged red and green fluorescence images are shown for ear; individual and merged images are shown for diaphragm. The same results were obtained in 6 repeat experiments (n = 6 mice). Original magnification, ×40 (**A**); ×100 (**B**).

are not apparent in this model. Conversely, mice deficient in the expression of one or more Ras isoforms develop lymphatic vessel hypoplasia and chylous ascites, also indicative of lymphatic vessel dysfunction (10). However, which RasGAPs regulate Ras signal transduction in lymphatic endothelial cells (LECs) has not to our knowledge been previously explored. Notably, a small number of CM-AVM patients also develop chylothorax and chylous ascites (9), which suggests that RASA1 may act as essential regulator of the lymphatic vasculature as well as the blood vasculature.

In this study, we sought to determine the function of RASA1 in tissue homeostasis in adult animals. We used a conditional RASA1-deficient mouse model, in which deletion of *Rasa1* in all tissues of adult mice occurs in response to drug administration (11). In these mice, induced deletion of *Rasa1* did not result in the development of spontaneous blood vascular lesions. Instead, a striking spontaneous disorder of the lymphatic vascular system resulted that was characterized by extensive lymphatic vessel dilation, hyperplasia, and leakage defects. These findings revealed an important role for RASA1 as a negative regulator of lymphatic vessel growth and function in unchallenged animals.

Results

Loss of RASA1 expression in adult mice does not result in the development of spontaneous blood vessel abnormalities. To examine the role played by RASA1 in adult tissues, we used mice that carry conditional floxed *Rasa1* alleles (*Rasa1*$^{fl/fl}$) and a ubiquitin promoter–driven Ert2Cre transgene (*Ub*^{ert2cre}) (11). Groups of *Rasa1*$^{fl/fl}$*Ub*^{ert2cre} and littermate control *Rasa1*$^{fl/fl}$ mice were given 2 i.p. injections of tamoxifen (TM) at 2 months of age. This treatment results in complete loss of RASA1 expression in all examined tissues, as assessed by Western blotting of whole organ lysates performed 1 week after TM induction (11). Given that RASA1 has been identified as a negative regulator of blood vessel angiogenesis in adult mice and that *RASA1* mutations cause CM-AVM in humans, we looked carefully for any evidence of spontaneous blood vascular abnormalities in TM-induced animals. However, no capillary or arteriovenous malformations were observed in any tissue, either upon gross examination or by whole mount staining of tissues with an anti-CD31 antibody (Figure 1A). A normal density of blood vessels was also observed by staining for SMA in tissue sections (see below).

To confirm that the *Ub*^{ert2cre} transgene and its protein product are active in blood vessels, we generated *Rosa26*^{eyfp} reporter *Ub*^{ert2cre} transgenic mice (12). Mice were administered TM at 2 months of age and again 10 days later. After a further 7 days, expression of yellow fluorescent protein (YFP) in blood vessels was shown to be strongly expressed by whole mount staining using anti-GFP and anti-CD31 antibodies (Figure 1B). In addition, loss of RASA1 expression in BECs was demonstrated directly by Western blotting (see below). Therefore, the absence of a spontaneous blood vessel phenotype in this model cannot be explained by the absence of *Rasa1* deletion in this vessel type.

In contrast to the above findings, constitutive loss of RASA1 expression during embryogenesis results in cardiovascular defects and lethality (5). To confirm that this phenotype is caused by loss of RASA1 in BECs specifically, we used the *Tie1-Cre* transgenic line to restrict expression of Cre to this lineage. Among progeny of crosses between *Rasa1*$^{fl/+}$*Tie1-Cre* and *Rasa1*$^{fl/fl}$ mice, no *Rasa1*$^{fl/fl}$*Tie1-Cre* pups were identified (Supplemental Figure 1A; supplemental material available online with this article; doi:10.1172/JCI46116DS1). Results of timed pregnancy experiments revealed that *Rasa1*$^{fl/fl}$*Tie1-Cre* embryos succumbed at E10–E11 as a result of defective cardiovascular development (Supplemental Figure 1B), similar to *Rasa1*-null embryos (5). Therefore, we concluded that RASA1 has a BEC-intrinsic function during blood vascular development.

Lymphatic vessel dysfunction in induced RASA1-deficient mice. We initially reported that induced RASA1-deficient mice remain healthy for 3 months after TM injection (11). However, when studies were

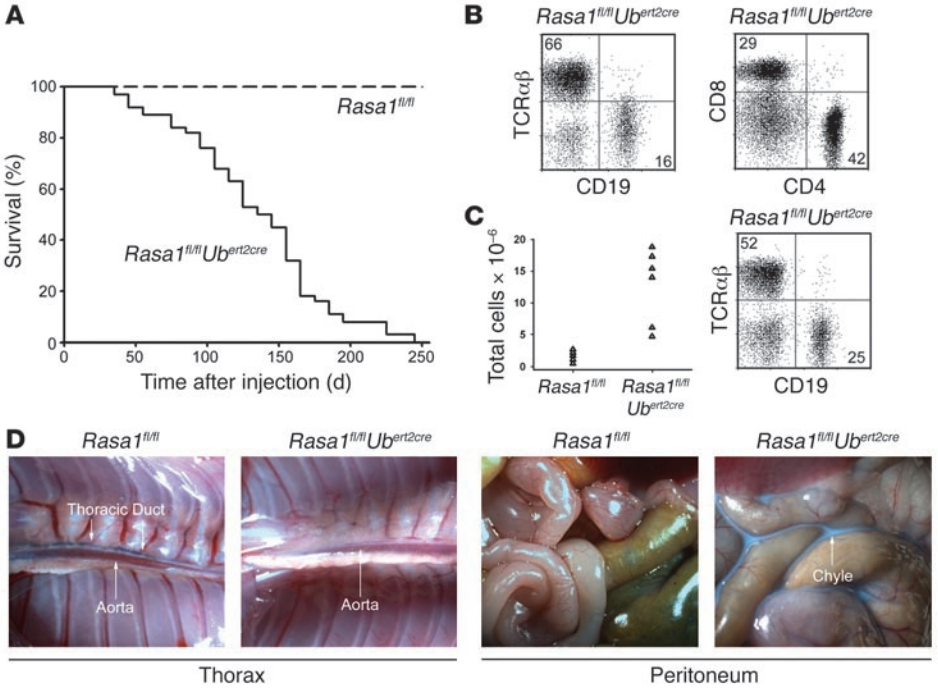

Figure 2

Induced loss of RASA1 expression in adult mice results in early mortality associated with chylothorax and chylous ascites. (**A**) Kaplan-Meier survival plots of *Rasa1*$^{fl/fl}$*Ub*^{ert2cre} and *Rasa1*$^{fl/fl}$ mice treated with TM at 2 months of age (n = 50 per genotype). (**B**) Flow cytometric analysis of pleural effusion cells from deceased TM-treated *Rasa1*$^{fl/fl}$*Ub*^{ert2cre} mice showing expression of lymphocytic markers TCRβ (T cells), CD4 (T cells), CD8 (T cells), and CD19 (B cells). Data are representative of 10 mice examined. (**C**) Total numbers and representative flow cytometric plot of peritoneal leukocytes obtained by lavage of *Rasa1*$^{fl/fl}$*Ub*^{ert2cre} and *Rasa1*$^{fl/fl}$ mice treated with TM 3 months prior (n = 6 per genotype). (**B** and **C**) Numbers in flow cytometry plots denote percent live cells. (**D**) Evans blue dye was injected s.c. into the hind footpads and tail of *Rasa1*$^{fl/fl}$*Ub*^{ert2cre} and *Rasa1*$^{fl/fl}$ mice treated with TM 3 months prior. Drainage of dye into the thoracic duct was examined 1 hour after injection. A blue thoracic duct was clearly visible in *Rasa1*$^{fl/fl}$ mice, but not *Rasa1*$^{fl/fl}$*Ub*^{ert2cre} mice; instead, in *Rasa1*$^{fl/fl}$*Ub*^{ert2cre} mice, injected dye commonly drained into the peritoneum. The same results were obtained in 5 repeat experiments.

extended, it became apparent that all *Rasa1*$^{fl/fl}$*Ub*^{ert2cre} mice succumbed by 8 months after TM administration (Figure 2A). Prior to death, mice frequently showed signs of labored breathing, and, upon necropsy, the thoracic cavity was filled with a milky white fluid with a high content of triglycerides (240–1,200 mg/dl; n = 7), much higher than that observed in serum. Flow cytometric analysis showed that the majority of cells in the effusion were lymphocytes (Figure 2B). Thus, the fluid had all the characteristics of chyle (lipid-laden lymph), accumulation of which in the thoracic cavity presumably suffocates mice, leading to death by chylothorax (13).

Leakage of lymph was not confined to the thoracic space in *Rasa1*$^{fl/fl}$*Ub*^{ert2cre} mice, since chyle was also commonly found in the peritoneal cavity (chylous ascites) of deceased animals. Furthermore, flow cytometric analysis of peritoneal flushes of groups of mice treated with TM 3 months previously consistently revealed the presence of large numbers of leukocytes, the majority of which were again lymphocytes (Figure 2C). These findings suggested that loss of RASA1 expression in adult mice results in a more general lymphatic leakage defect. To confirm this, we performed Evans blue tracing studies. Mice treated with TM 3 months prior were injected with Evans blue in the hind footpads and tail. After 1 hour, mice were euthanized, and drainage of dye into the thoracic duct was examined (Figure 2D). In TM-treated *Rasa1*$^{fl/fl}$ mice, dye was readily detected in the thoracic duct, to which it gains access via the cisternae chyli. In contrast, in TM-treated *Rasa1*$^{fl/fl}$*Ub*^{ert2cre} mice, drainage of dye to the thoracic duct was never observed; instead, dye commonly leaked into the peritoneal cavity of mice, presenting as blue chyle (Figure 2D).

Lymphatic vessel dilation and development of extensive lymphatic vessel hyperplasia in induced RASA1-deficient mice. Chylothorax, which occurs perinatally, has been reported in some other mutant mouse models (14–17). In these models, chylothorax is often associated with dilation of thoracic lymphatic vessels. To determine whether thoracic lymphatic vessels of induced RASA1-deficient mice also show evidence of dilation, we performed immunohistochemical studies of the chest region using a lymphatic-specific LYVE-1 antibody (Figure 3, A and B, and ref. 18). Lymphatic vessels of the chest wall were indeed markedly dilated in *Rasa1*$^{fl/fl}$*Ub*^{ert2cre} mice. However, more striking was the observed large increase in the density of lymphatic vessels both within the chest wall and on the inside of the chest wall facing the pleural cavity. In control mice, lymphatic vessels were scarce on the inside of the chest wall, whereas in *Rasa1*$^{fl/fl}$*Ub*^{ert2cre} mice, there was almost continuous coverage of the pleural face of the chest wall with lymphatic vessels (Figure 3B). The identity of these vessels as lymphatic was confirmed by their expression of VEGF receptor 3 (VEGFR-3) in double immunofluorescence staining experiments (Supplemental Figure 2).

Lymphatic vessel dilation and hyperplasia was also observed in other tissues of TM-treated *Rasa1*$^{fl/fl}$*Ub*^{ert2cre} mice. In skin, hyperplasia was readily apparent after i.d. injection of shaved mice with

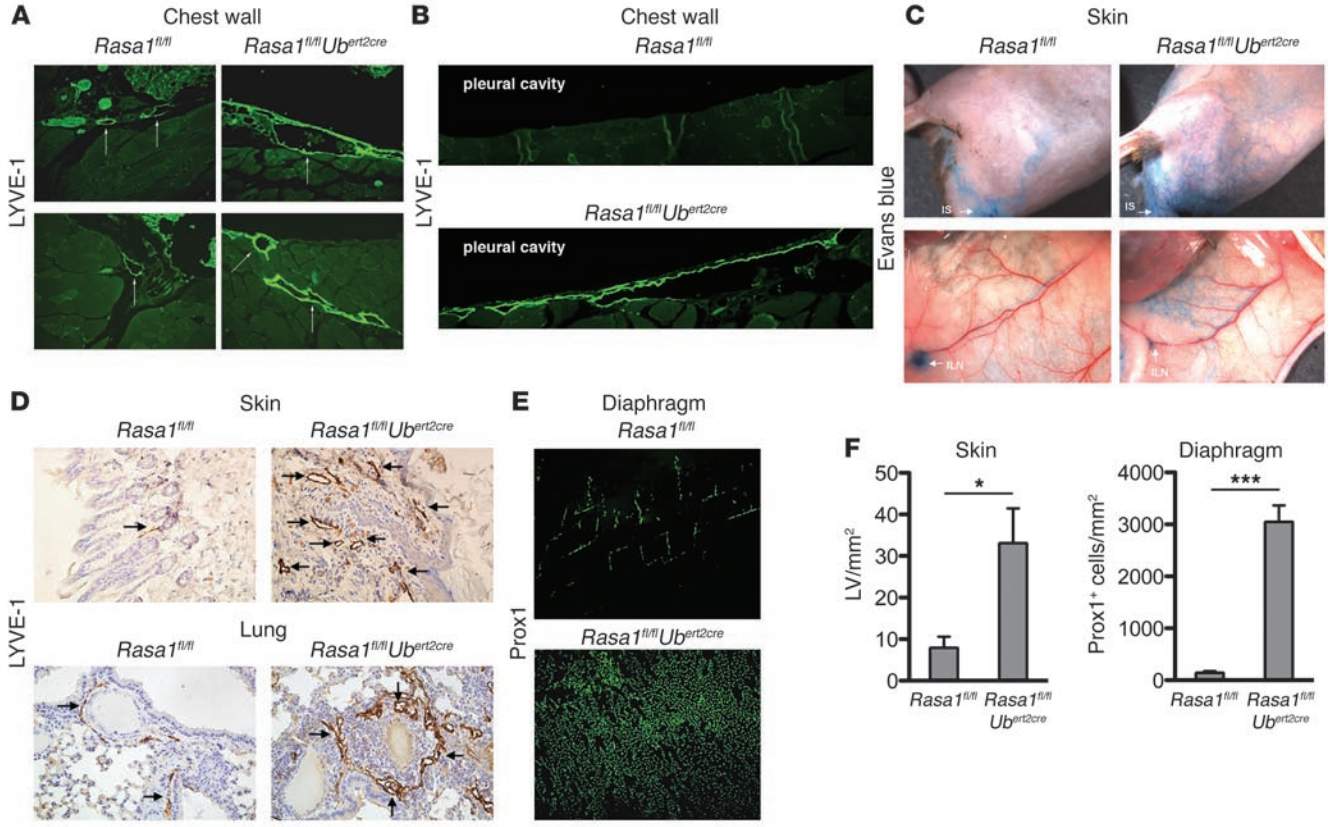

Figure 3

Lymphatic vessel dilation and hyperplasia in induced RASA1-deficient mice. (**A** and **B**) Anti–LYVE-1 antibody–stained sections of the chest wall of *Rasa1*$^{fl/fl}$*Ub*^{ert2cre} and *Rasa1*$^{fl/fl}$ mice treated with TM 4 months prior (n = 25 per genotype). (**A**) Arrows denote representative lymphatic vessels within the chest wall. (**B**) Lower-power composite images. (**C**) Evans blue was injected i.d. at the base of the tail of shaved *Rasa1*$^{fl/fl}$*Ub*^{ert2cre} and *Rasa1*$^{fl/fl}$ mice treated with TM 4 months prior. The dermal lymphatic network draining the injection site (IS) was imaged after 1 minute (top). After 5 minutes, a midline incision was made to expose lymphatic vessels and the inguinal LN (ILN) on the underside of the skin (bottom). The experiment was repeated 3 times with the same findings. (**D**) Representative anti–LYVE-1 antibody–stained sections of skin and lung of *Rasa1*$^{fl/fl}$*Ub*^{ert2cre} and *Rasa1*$^{fl/fl}$ mice (n = 6 per genotype) treated with TM 3 months prior. Arrows denote lymphatic vessels. (**E**) Representative whole mount anti-Prox1 antibody staining of diaphragms of *Rasa1*$^{fl/fl}$*Ub*^{ert2cre} and *Rasa1*$^{fl/fl}$ mice treated with TM 4 months prior (n = 5 per genotype). (**F**) Number of lymphatic vessels (LV) or Prox1$^+$ cells per mm^2 in skin and diaphragms, respectively, of *Rasa1*$^{fl/fl}$*Ub*^{ert2cre} and *Rasa1*$^{fl/fl}$ mice in **D** and **E**. Data (mean + 1 SEM) were derived from 6 randomly selected fields from 3 mice per genotype. $^*P < 0.05$; $^{***}P < 0.001$. Original magnification, ×400 (**A**); ×40 (**B**); ×100 (**D** and **E**).

Evans blue dye at the base of the tail (Figure 3C). As detected by anti–LYVE-1 immunohistochemical staining, lymphatic vessels in skin and lung were dilated and increased in number (Figure 3D). Furthermore, immunofluorescence staining of whole mount diaphragms using an antibody against the Prox1 LEC transcription factor revealed a very large increase in the number of LECs in *Rasa1*$^{fl/fl}$*Ub*^{ert2cre} mice (Figure 3E). Quantitative analysis of skin and diaphragm confirmed the increased density of lymphatic vessels in *Rasa1*$^{fl/fl}$*Ub*^{ert2cre} mice (Figure 3F).

Dynamic imaging of lymph flow in induced RASA1-deficient mice. To study the lymphatic defect in induced RASA1-deficient mice further, we performed dynamic noninvasive near-infrared (NIR) fluorescence imaging studies of lymph flow in live mice (19, 20). TM-treated *Rasa1*$^{fl/fl}$*Ub*^{ert2cre} mice and *Rasa1*$^{fl/fl}$ controls were injected with indocyanine green (ICG) i.d. at the base of the tail. Fluorescence images of mice were then acquired for up to 20 minutes (Figure 4 and Supplemental Videos 1 and 2). These analyses provided noninvasive confirmation of the extensive lymphatic hyperplasia in induced RASA1-deficient mice. In control mice, dye followed an almost direct route of drainage from the site of injection to the inguinal LN, and subsequently to the axillary LN, via an inguinal-to-axillary internodal lymphatic vessel (INL). However, in induced RASA1-deficient mice, dye first entered into an expansive lymphatic vessel network before drainage to the INL (Figure 4). Another striking feature of the induced RASA1-deficient mice was that numerous lymphatic vessels were seen to branch off from the INL. We have not observed such lymphatic vessel sprouting from this lymphatic channel in control mice. Longitudinal NIR fluorescence imaging of induced RASA1-deficient mice revealed that lymphatic hyperplasia was first apparent at 2–3 weeks after TM administration. Thereafter, the extent of hyperplasia increased progressively, reaching a maximum at 8 weeks after TM treatment (Supplemental Figure 3).

For several selected regions of interest (ROIs) within the lymphatic network of induced RASA1-deficient and control mice, we analyzed fluorescence intensity with respect to time (Figure 4B). These studies revealed an absence of pulsatile activity in the hyper-

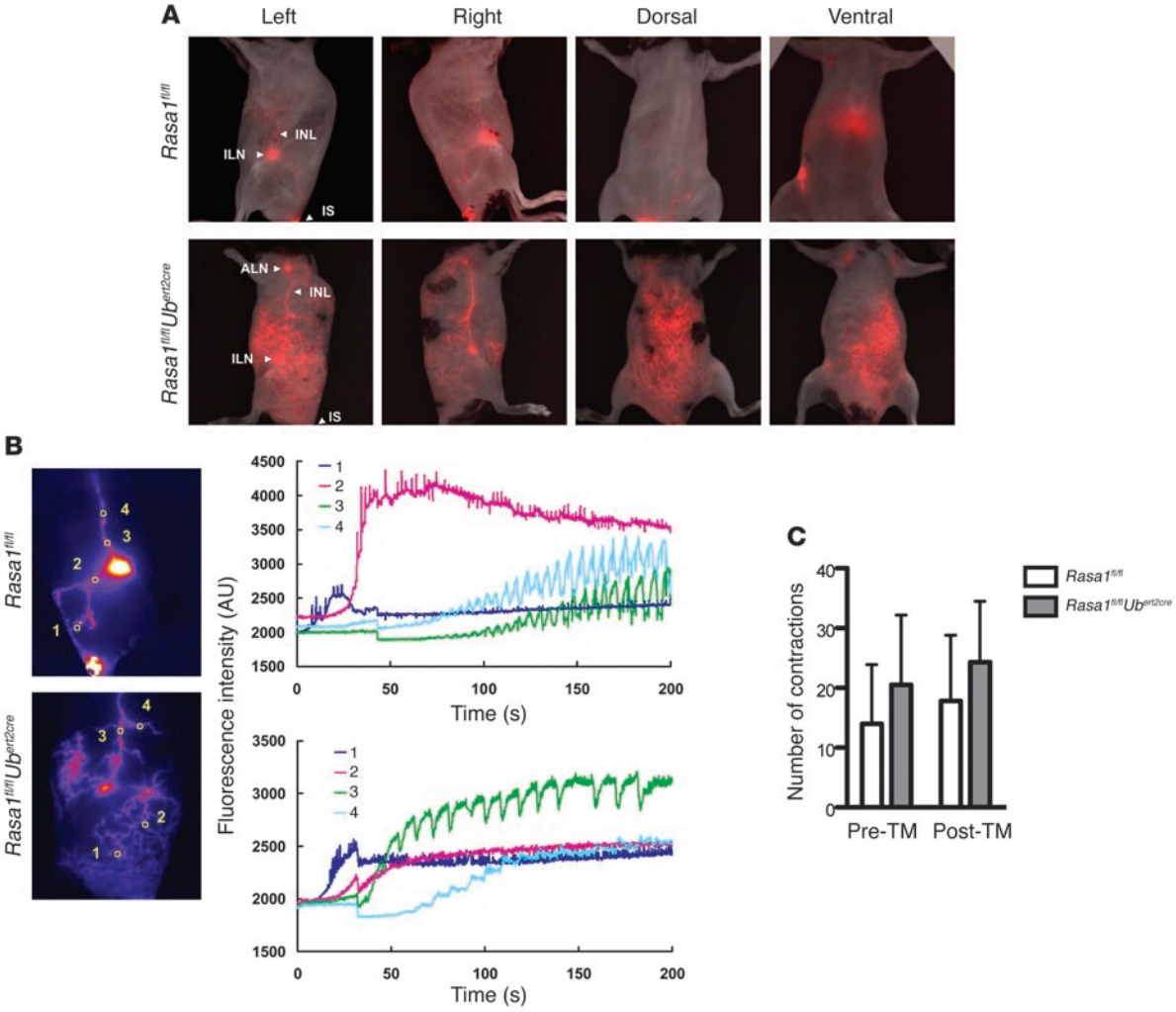

Figure 4

Quantitative analysis of propulsive lymph function in induced RASA1-deficient mice. (**A**) *Rasa1*$^{fl/fl}$*Ub*^{ert2cre} and *Rasa1*$^{fl/fl}$ mice treated with TM 3–4 months prior were injected i.d. at the base of the tail with ICG. Shown are fluorescence images superimposed on white-light images of live animals taken 20 minutes after ICG injection, revealing dermal lymphatic networks. (**B**) Fluorescence images of mice in **A** acquired 3 minutes after ICG injection. Numbers denote select ROIs within the lymphatic network, and their fluorescence intensities with respect to time after injection are shown. ROI 1 and ROI 2 in both groups, lymphatic vessels draining the site of injection; ROI 3 in both groups and ROI 4 in *Rasa1*$^{fl/fl}$, INL collecting lymphatic vessels; ROI 4 in *Rasa1*$^{fl/fl}$*Ub*^{ert2cre}, newly formed lymphatic vessels that branch off from the INL. The same results were obtained with all other examined *Rasa1*$^{fl/fl}$*Ub*^{ert2cre} and *Rasa1*$^{fl/fl}$ control mice (n = 10 of each genotype). See also Supplemental Figure 3 and Supplemental Videos 1 and 2. (**C**) Number of contractions over a 5-minute period in INL of *Rasa1*$^{fl/fl}$*Ub*^{ert2cre} and *Rasa1*$^{fl/fl}$ mice before and after TM injection. Measurements were initiated 5 minutes after ICG injection (n = 6 per genotype). Data are mean + 1 SEM. Differences were not statistically significant.

plastic draining lymphatics proximal to the site of injection in induced RASA1-deficient mice. This is consistent with their identity as lymphatic capillaries or newly formed lymphatic vessels that lack the smooth muscle cell coverage associated with more mature vessels (18). Likewise, there was an absence of pulsatile activity in lymphatic vessels that branched off from the INL in induced RASA1-deficient mice. Pulsatile activity was detected in larger collecting lymphatic vessels of induced RASA1-deficient mice; however, the propulsive rates in these larger vessels were on average not different from those in control mice (Figure 4C). Thus, even though there is lymphatic vessel hyperplasia in induced RASA1-deficient mice, there does not appear to be loss of vessel lymph-propelling ability. This is in agreement with the absence of any evidence of tissue lymphedema in this model.

Lack of smooth muscle coverage of the majority of lymphatic vessels in induced RASA1-deficient mice. In parallel with our NIR fluorescence imaging studies, we examined whether newly formed lymphatic vessels in induced RASA1-deficient mice are invested with smooth muscle. Tissue sections of chest wall, skin, and esophagus were double stained with anti–LYVE-1 and anti-SMA antibodies (Figure 5). The vast majority of lymphatic vessels in induced RASA1-deficient mice were not invested with smooth muscle. This finding is consistent with the lack of contractile activity in the majority of lymphatic vessels in these animals, as shown by NIR fluorescence imaging (Figure 4).

Induced loss of RASA1 in lymphatic endothelial cells is sufficient to cause lymphatic vessel dilation and hyperplasia. The early onset of lymphatic vessel hyperplasia (Supplemental Figure 3) and the fact that tissue lymphedema is not observed in induced RASA1-deficient mice

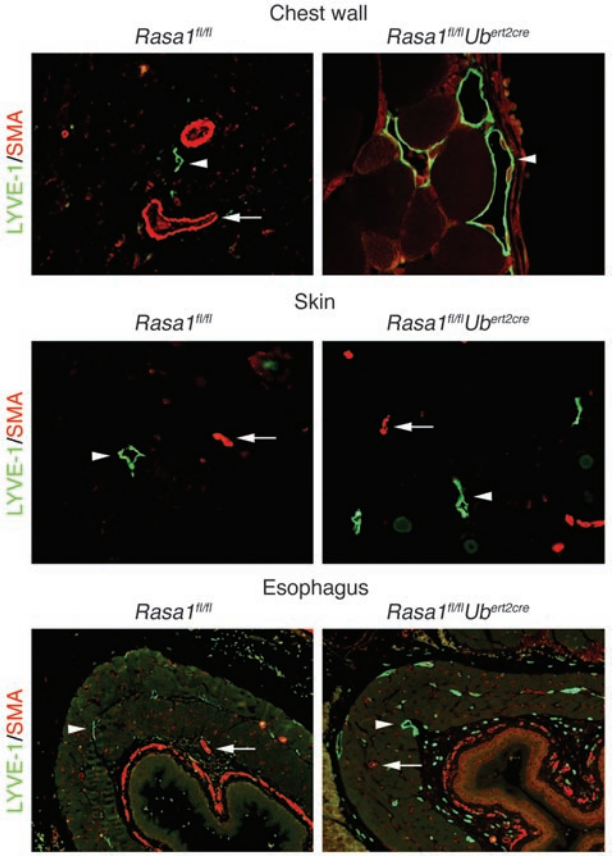

Figure 5
The majority of newly formed lymphatic vessels in induced RASA1-deficient mice do not have smooth muscle coverage. Sections of chest wall, skin, and esophagus from *Rasa1*$^{fl/fl}$*Ub*^{ert2cre} and *Rasa1*$^{fl/fl}$ mice treated with TM 3–4 months prior were stained with anti–LYVE-1 (green) and anti-SMA (red) antibodies. Some lymphatic vessels (arrowheads) and blood vessels (arrows) are indicated. Original magnification, ×100 (chest wall and skin); ×40 (esophagus).

both argue strongly against the notion that the increased number of lymphatics arises as part of a homeostatic response to lymphatic vessel leakage. Instead, we hypothesized that increased LEC proliferation is the primary cause of the increased number of vessels. This could be consequent to increased production of LEC growth factors in RASA1-deficient mice causing elevated steady-state concentrations of growth factors in tissues. Alternatively, lymphatic vessel abnormalities could be caused by dysregulated LEC growth factor receptor signaling in response to low concentrations of growth factors in the extracellular milieu. As determined by RT-PCR, no difference in the expression of a number of LEC growth factors — including FGF, PDGF, VEGF-C (the ligand for VEGFR-3), and angiopoietin 1 — was detected in any tissue derived from induced RASA1-deficient mice (data not shown and ref. 18). Therefore, to obtain evidence for the alternative hypothesis, we first asked whether the lymphatic vessel phenotype could result from loss of RASA1 specifically in LECs. We used the recently described *Prox1*^{ert2cre} knockin line, in which the Prox1 promoter drives expression of Ert2Cre (21). To confirm that TM-inducible Cre activity was restricted to lymphatic vessels in this line, we generated *Rosa26*^{eyfp}*Prox1*^{ert2cre} mice. After 3 repeat injections of TM, YFP protein expression was detected in lymphatic vessels, but not blood vessels, of these mice (Figure 6A). We further examined whether Ert2Cre is active in both initial and collecting lymphatic vessels in *Prox1*^{ert2cre} mice. In *Rosa26*^{eyfp}*Prox1*^{ert2cre} mice, YFP was expressed within initial lymphatic vessels of the central diaphragm (Figure 6B), which were clearly identified by the oak-leaf appearance of the LECs therein (22). Similarly, YFP was expressed in collecting lymphatic vessels enriched in the peripheral diaphragm (Figure 6B), identified by the spindle-like appearance of LECs (22). Of note, however, in *Rosa26*^{eyfp}*Prox1*^{ert2cre} mice, YFP was expressed in a relative minority of LECs in initial and collecting lymphatic vessels. Conversely, in *Rosa26*^{eyfp}*Ub*^{ert2cre} mice, YFP was expressed in all LECs of initial and collecting lymphatic vessels (Figure 6B).

Lymphatic vessel–specific inducible RASA1-deficient *Rasa1*$^{fl/fl}$*Prox1*^{ert2cre} mice were generated by intercrossing *Rasa1*$^{fl/fl}$ and *Prox1*^{ert2cre} mice. TM was administered to mice and to *Rasa1*$^{fl/fl}$ littermate controls at 2 months of age; 3 months later, mice were analyzed for lymphatic vessel abnormalities. As shown by LYVE-1 immunohistochemical staining, lymphatic vessels in skin of *Rasa1*$^{fl/fl}$*Prox1*^{ert2cre} mice were dilated and increased in number to an extent similar to that observed in *Rasa1*$^{fl/fl}$*Ub*^{ert2cre} mice (Figure 7, A and C, and Figure 3, D and F). In addition, in whole mount diaphragm specimens, a large increase in Prox1$^+$ cell numbers was observed in *Rasa1*$^{fl/fl}$*Prox1*^{ert2cre} mice, albeit not as large as that in *Rasa1*$^{fl/fl}$*Ub*^{ert2cre} mice (Figure 7, B and C, and Figure 3, E and F).

We also examined lymphatic vessel structure and flow in *Rasa1*$^{fl/fl}$*Prox1*^{ert2cre} mice by NIR fluorescence imaging (Figure 7D and Supplemental Videos 3 and 4). Dermal lymphatic vessel hyperplasia was readily observed in *Rasa1*$^{fl/fl}$*Prox1*^{ert2cre} mice. Longitudinal NIR fluorescence imaging of *Rasa1*$^{fl/fl}$*Prox1*^{ert2cre} mice revealed that the lymphatic vessel hyperplastic phenotype was first apparent 2–3 weeks after TM treatment, similar to *Rasa1*$^{fl/fl}$*Ub*^{ert2cre} mice (data not shown).

Induced lymphatic vessel–specific loss of RASA1 during development results in chylothorax in weanling mice. In contrast to *Rasa1*$^{fl/fl}$*Ub*^{ert2cre} mice, no early lethality was noted in *Rasa1*$^{fl/fl}$*Prox1*^{ert2cre} mice, and these mice showed no evidence of chylothorax or chylous ascites up to 1 year after TM injection (n = 30). This finding could indicate that, in contrast to lymphatic vessel hyperplasia, lymphatic leakage resulting from systemic loss of RASA1 in adults is not caused by loss of RASA1 in LECs. However, in adult mice, *Prox1*^{ert2cre} caused detectable recombination in a minority of LECs in lymphatic vessels (Figure 6), which could account for the absence of overt signs of lymphatic vessel leakage. To address this, we administered TM to pregnant *Rasa1*$^{fl/fl}$ dams carrying *Rasa1*$^{fl/fl}$*Prox1*^{ert2cre} and *Rasa1*$^{fl/fl}$ control embryos at E15. Our rationale was that, since all LECs in adult mice must descend from Prox1$^+$ LEC progenitors, then earlier administration of TM during development should result in more effective deletion of *Rasa1* in LECs in adult mice (23, 24). Indeed, TM administration at E15 resulted in chylothorax and death of *Rasa1*$^{fl/fl}$*Prox1*^{ert2cre} mice 2 weeks after birth (Figure 7, E and F). Half of the *Rasa1*$^{fl/fl}$*Prox1*^{ert2cre} mice developed chylothorax, whereas chylothorax was not observed in any *Rasa1*$^{fl/fl}$ littermate controls.

Increased circumferential growth and LEC proliferation in induced RASA1-deficient mice. As confirmed by double staining with anti–LYVE-1 and anti-Prox1 antibodies or with antibodies against Prox1 and the intercellular adhesion molecule VE-cadherin, lymphatic vessels in TM-treated *Rasa1*$^{fl/fl}$*Ub*^{ert2cre} and *Rasa1*$^{fl/fl}$*Prox1*^{ert2cre} mice showed large increases in circumferential growth (Figure 8, A and B). To confirm that increased LEC number and vessel growth are

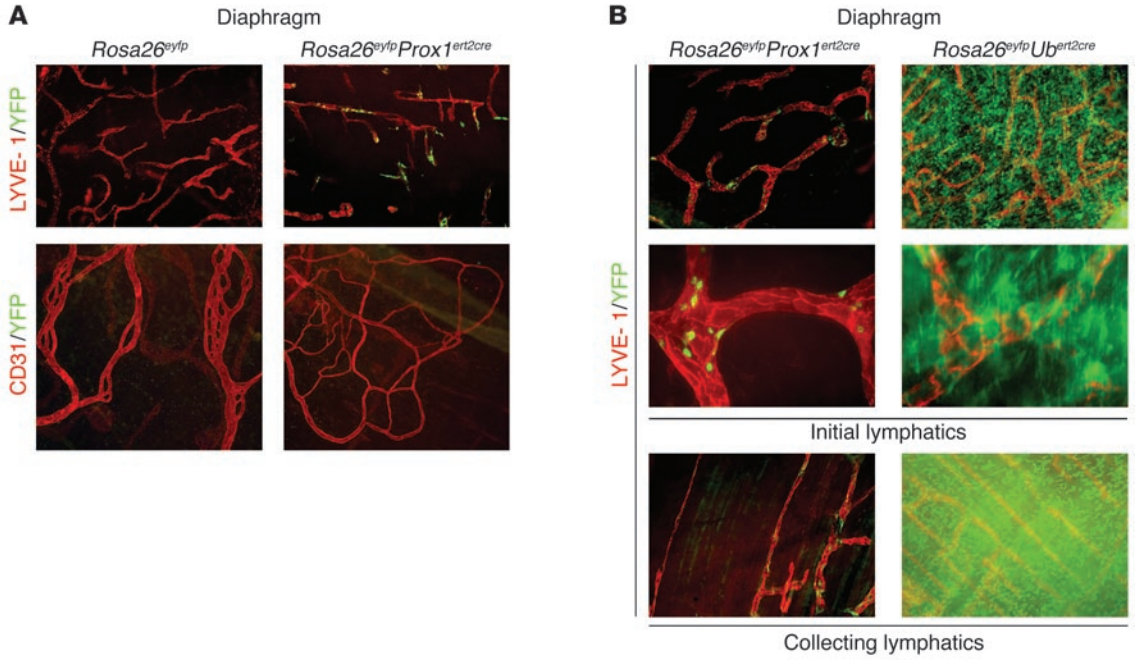

Figure 6

Cre-mediated recombination in *Prox1*^{ert2cre} mice. (**A**) Adult *Rosa26*^{eyfp} and *Rosa26*^{eyfp}*Prox1*^{ert2cre} mice were administered TM at 2 months of age. Repeat TM injections were given 10 and 20 days later. 7 days after the last TM injection, whole mount diaphragm specimens were stained with anti-GFP antibodies (green) to identify sites of YFP expression and with anti–LYVE-1 or anti-CD31 antibodies (red) to identify lymphatic vessels and blood vessels, respectively. Images were taken from the central part of the diaphragm. (**B**) Adult *Rosa26*^{eyfp}*Prox1*^{ert2cre} mice and *Rosa26*^{eyfp}*Ub*^{ert2cre} mice were administered TM as described in **A** and Figure 1, respectively. 7 days after the last injection, whole mount diaphragm specimens were stained with anti–LYVE-1 (red) and anti-GFP (green) antibodies. In initial lymphatics, expression was enriched in the central diaphragm; in collecting lymphatics, expression was more commonly observed in the peripheral diaphragm. Similar results were obtained in 5 different mice per genotype. Original magnification, ×40 (**A**, LYVE-1, and **B**, initial lymphatics [top] and collecting lymphatics); ×100 (**A**, CD31, and **B**, initial lymphatics [bottom]).

consequences of increased LEC proliferation, we performed in vivo BrdU labeling experiments. Adult *Rasa1*$^{fl/fl}$*Ub*^{ert2cre} mice were injected with BrdU 8 and 10 days after TM administration. At 2 hours after the second BrdU injection, whole mount diaphragms were stained with anti–LYVE-1 and anti-BrdU antibodies (Figure 8C). At this early time point after TM administration, numerous lymphatic vessel sprouts were observed in *Rasa1*$^{fl/fl}$*Ub*^{ert2cre} mice, but not in *Rasa1*$^{fl/fl}$ mice. Moreover, in *Rasa1*$^{fl/fl}$*Ub*^{ert2cre} mice, BrdU^{+} nuclei were detected in the vicinity of these sprouts (Figure 8C). Under the labeling conditions used, BrdU^{+} nuclei were not identified in *Rasa1*$^{fl/fl}$ mice.

To more reliably quantify differences in LEC proliferation, we performed combined in vivo BrdU labeling and ex vivo flow cytometric staining analyses. *Rasa1*$^{fl/fl}$*Ub*^{ert2cre} mice were injected with BrdU 3 and 5 days after TM administration. At 2 hours after the last BrdU dose, whole lung cell suspensions were prepared and stained with anti-CD45, anti-podoplanin, anti-CD31, and anti-BrdU antibodies. Within whole lung cell preparations, LECs were identified as CD45^{-}podoplanin^{+}CD31^{lo} and were readily distinguished from BECs, identified as CD45^{-}podoplanin^{-}CD31^{+} (Figure 8D and ref. 18). Consistent with the identity of this population as LECs, cells expressed LYVE-1 and VEGFR-3 (data not shown). Importantly, comparison of LECs from TM-induced *Rasa1*$^{fl/fl}$*Ub*^{ert2cre} and *Rasa1*$^{fl/fl}$ mice revealed an approximately 6-fold increase in BrdU incorporation in the former (Figure 8D). These findings support the notion that lymphatic vessel hyperplasia in induced RASA1-deficient mice results from increased LEC proliferation. Conversely, no increase in BrdU incorporation into BECs was noted in TM-induced *Rasa1*$^{fl/fl}$*Ub*^{ert2cre} mice compared with controls (Figure 8D). This finding is consistent with the absence of a spontaneous blood vascular phenotype in these mice.

RASA1-deficient LECs show dysregulated Ras signal transduction initiated through multiple LEC growth factor receptors. As revealed by staining of serial sections of the chest wall with anti–LYVE-1 and anti–phospho-MAPK antibodies, the Ras-MAPK pathway was commonly activated in LECs from TM-induced *Rasa1*$^{fl/fl}$*Ub*^{ert2cre} mice (Figure 9A). In contrast, activation of the Ras-MAPK pathway in LECs of control *Rasa1*$^{fl/fl}$ mice was not observed. This observation is consistent with a model in which the loss of RASA1 in LECs allows low levels of growth factors present in the extracellular space of resting animals to trigger activation of the Ras-MAPK pathway and abnormal downstream LEC proliferation.

To determine which LEC growth factor receptors might have become dysregulated in LECs upon loss of RASA1, we conducted in vitro signaling experiments. LECs were isolated from lungs of *Rasa1*$^{fl/fl}$*Ub*^{ert2cre} and *Rasa1*$^{fl/fl}$ mice treated with TM 2 weeks prior by positive selection from whole lung cell suspensions using an anti-podoplanin antibody (25). Cells were then expanded for 5–7 days in medium containing endothelial cell growth supplement (ECGS) before assay. This procedure yielded essentially pure LEC populations that uniformly expressed VEGFR-3 and were not contaminated with epithelial cells (Supplemental Figure 4A). Western blotting confirmed that RASA1 was not expressed in purified LECs from *Rasa1*$^{fl/fl}$*Ub*^{ert2cre} mice (Supplemental Figure 4B).

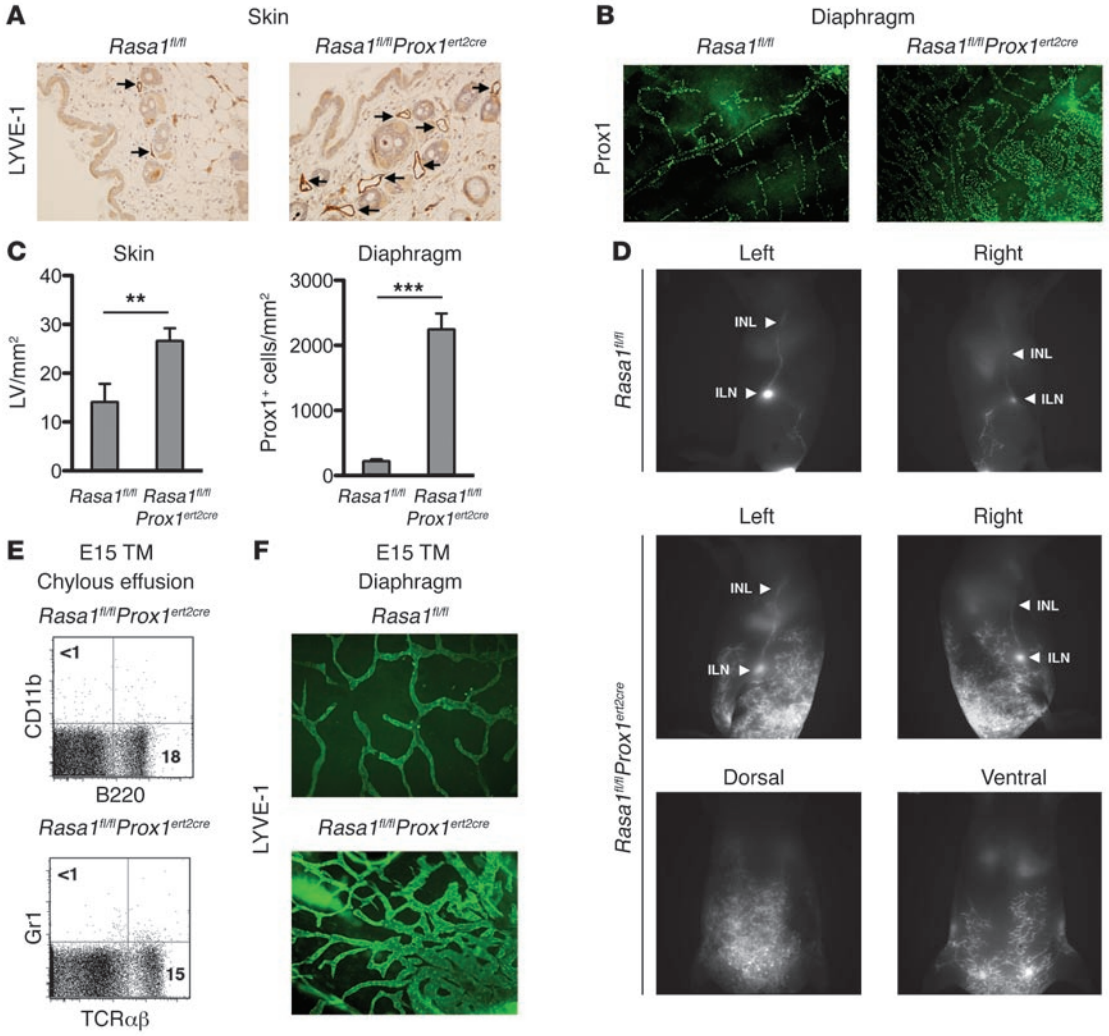

Figure 7

Lymphatic vessel hyperplasia and chylothorax in LEC-specific induced RASA1-deficient mice. (**A** and **B**) Skin sections and whole mount diaphragms from *Rasa1*$^{fl/fl}$*Prox1*^{ert2cre} and *Rasa1*$^{fl/fl}$ mice injected with TM 3 months prior (at 2 months of age) were stained with anti–LYVE-1 and anti-Prox1 antibodies, respectively, to identify lymphatic vessels (arrows in **A**). (**C**) Number of lymphatic vessels and Prox1$^+$ cells per mm^2 in skin and diaphragms, respectively, of mice in **A** and **B**. Data (mean + 1 SEM) were derived from 6 randomly selected fields from 3 mice per genotype. $^{**}P < 0.01$; $^{***}P < 0.001$. (**D**) ICG was injected i.d. at the base of the tail of *Rasa1*$^{fl/fl}$*Prox1*^{ert2cre} and *Rasa1*$^{fl/fl}$ mice injected with TM 3 months prior (at 2 months of age). Representative fluorescence images were acquired 30 minutes later ($n = 5$ per genotype; see also Supplemental Videos 4 and 5). (**E**) Pleural effusions of deceased (2 weeks after birth) *Rasa1*$^{fl/fl}$*Prox1*^{ert2cre} mice administered TM at E15 were analyzed by flow cytometry for expression of lymphocytic (TCRβ, T cell; B220, B cell) and myeloid (CD11b and Gr1) markers. Numbers in quadrants indicate percent live cells. Note the abundant lymphocytes, but absent myeloid cells. (**F**) Whole mount diaphragm specimens from deceased *Rasa1*$^{fl/fl}$*Prox1*^{ert2cre} mice in **E** and littermate *Rasa1*$^{fl/fl}$ controls (euthanized at 2 weeks of age) were stained with an anti–LYVE-1 antibody to confirm lymphatic vessel hyperplasia. Original magnification, ×100 (**A** and **F**); ×40 (**B**).

We examined Ras signal transduction initiated by PDGF, FGF, and VEGF-C. Purified LECs were stimulated with growth factors for different times up to 2 hours. Activation of the Ras pathway was then assessed by Western blotting using phospho-MAPK antibodies (Figure 9B). For PDGF and FGF, the MAPK response was slightly prolonged in RASA1-deficient LECs. A more marked difference, however, was observed for VEGF-C. In control LECs, the peak VEGF-C–induced MAPK response occurred at 3 minutes. Similarly, in RASA1-deficient LECs, an early peak of MAPK activation was observed at 3 minutes, before a return to baseline levels of activation at 10 minutes. However, in RASA1-deficient LECs, a second wave of MAPK activation occurred 1 hour after stimulation that was maintained for at least an hour. VEGF-C also interacts with VEGFR-2 as well as VEGFR-3 (18). Therefore, to distinguish between dysregulated signal transduction through VEGFR-3 versus VEGFR-2, we also examined Ras-MAPK activation triggered by VEGF-A, which binds to VEGFR-1 and VEGFR-2 (18). No difference in the magnitude or kinetics of the VEGF-A–induced MAPK response was observed between RASA1-deficient and control LECs. Therefore, dysregulated Ras signal transduction is specific to VEGFR-3. Differences in the kinetics of Ras signal transduction induced by FGF, PDGF, and VEGFR-3

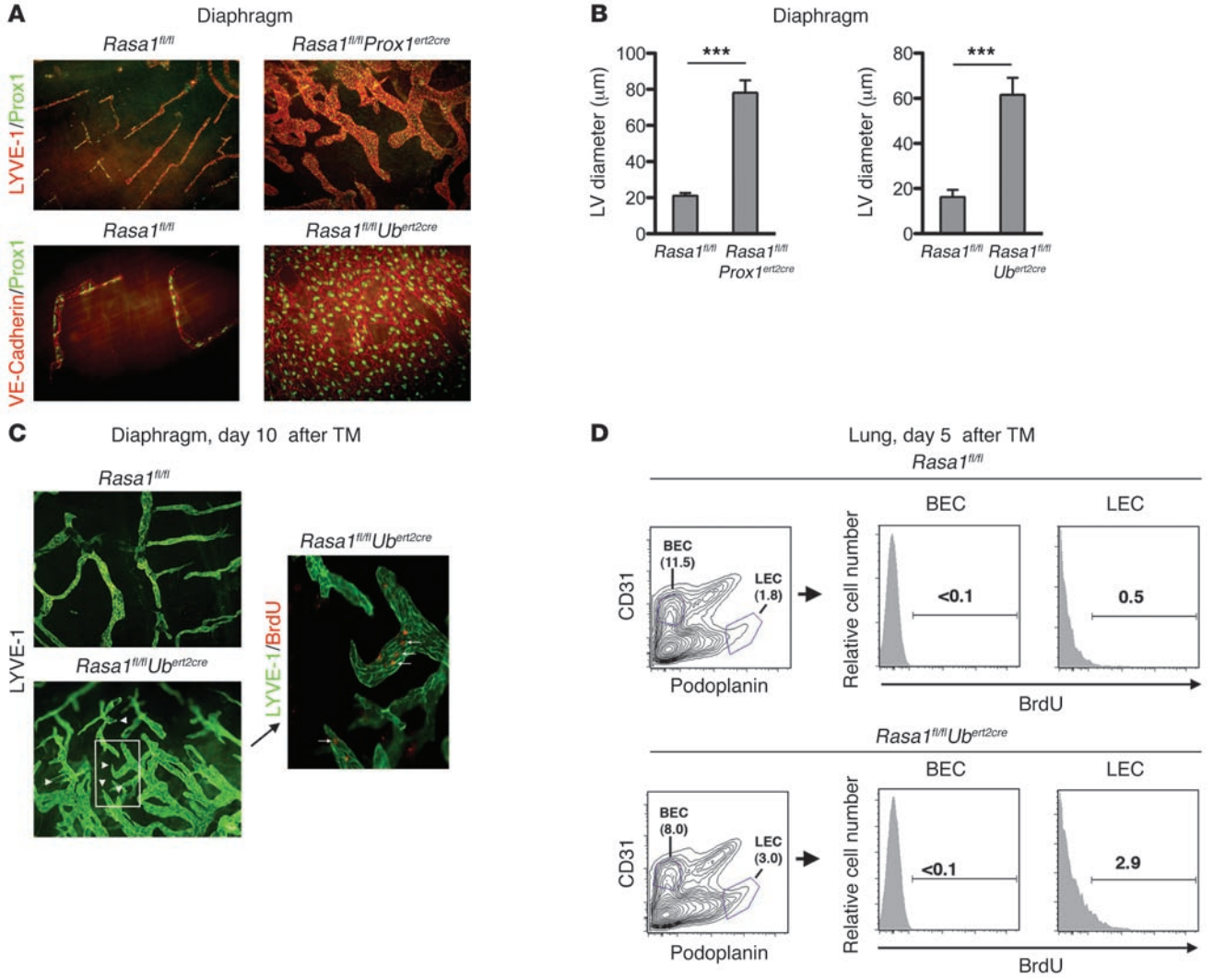

Figure 8

Lymphatic vessel growth in vivo in induced RASA1-deficient mice. (**A**) Whole mount diaphragms from *Rasa1*$^{fl/fl}$*Prox1*^{ert2cre}, *Rasa1*$^{fl/fl}$*Ub*^{ert2cre}, and *Rasa1*$^{fl/fl}$ mice injected with TM 3 months prior were stained with anti–LYVE-1 or anti–VE-cadherin antibodies (red) and anti-Prox1 antibodies (green). (**B**) Lymphatic vessel diameter in diaphragms of mice in **A**. Data (mean + 1 SEM) are derived from 6 randomly selected fields from 3 mice per genotype. ***$P < 0.001$. (**C**) *Rasa1*$^{fl/fl}$*Ub*^{ert2cre} and *Rasa1*$^{fl/fl}$ mice were administered TM at 2 months of age, then BrdU 8 and 10 days later. 2 hours after the last BrdU dose, whole mount diaphragms were stained with anti–LYVE-1 and anti-BrdU antibodies. Note the numerous lymphatic sprouts (arrowheads) and BrdU$^+$ nuclei (arrows) in *Rasa1*$^{fl/fl}$*Ub*^{ert2cre} mice. Images are representative of 3 mice per genotype. The boxed region is shown enlarged 3-fold. (**D**) *Rasa1*$^{fl/fl}$*Ub*^{ert2cre} and *Rasa1*$^{fl/fl}$ mice were administered TM at 2 months, then BrdU 3 and 5 days later. 2 hours after the last BrdU injection, whole lung cell suspensions were analyzed by flow cytometry. Shown are representative 2-color plots of podoplanin versus CD31 staining on gated CD45$^-$ cells (blue gates denote LEC and BEC populations) and BrdU staining within LECs and BECs. Numbers indicate percent representation among total live cells in each plot. Similar results were obtained in 2 repeat experiments. Original magnification, ×100 (**A**, top); ×400 (**A**, bottom, and **C**).

could not be explained by any alterations in the expression levels of respective receptors upon LECs. Thus, RASA1-deficient and control LECs expressed the same levels of VEGFR-3, as determined by flow cytometry (Supplemental Figure 4A), and the same levels of PDGFR and FGFR-3 (the principal FGFR expressed by LECs), as determined by Western blotting (Supplemental Figure 4B, data not shown, and ref. 26).

In the same experiments, we additionally examined activation of the AKT kinase, which also lies downstream of Ras and which promotes cell survival (Figure 9B and ref. 27). FGF and VEGF-A did not induce activation of AKT in either type of LEC (data not shown). PDGF did activate AKT, although no significant differences in the kinetics of AKT activation were apparent between control and RASA1-deficient LECs (Figure 9B). In contrast, major differences in AKT activation were noted when LECs were stimulated with VEGF-C. Thus, AKT activation was observed at an early time point (1–3 minutes) in both types of LECs, but only in RASA1-deficient LECs was a second wave of AKT activation observed, first detected at 1 hour after stimulation and again maintained for at least an additional hour (Figure 9B).

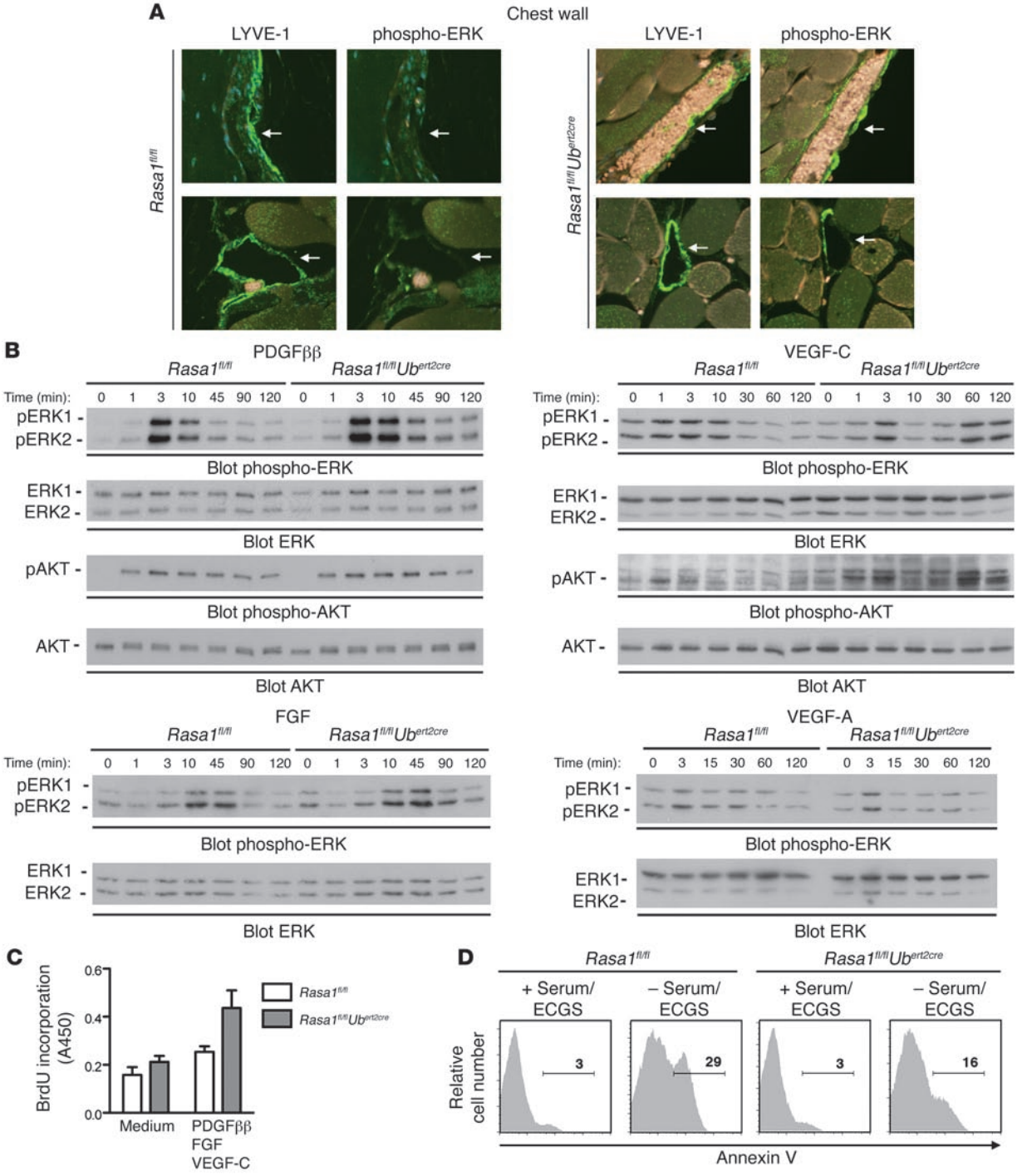

Figure 9

Dysregulated Ras signal transduction in RASA1-deficient LECs. (**A**) Serial sections of the chest wall of *Rasa1*$^{fl/fl}$*Ub*^{ert2cre} and *Rasa1*$^{fl/fl}$ mice treated with TM 4 months prior were stained with anti–LYVE-1 or anti–phospho-ERK antibody. Arrows denote lymphatic vessels. Images are representative of 4 examined mice per genotype. Original magnification, ×100. (**B**) LECs were isolated from lungs of *Rasa1*$^{fl/fl}$*Ub*^{ert2cre} and *Rasa1*$^{fl/fl}$ mice treated with TM 2 weeks prior (see Supplemental Figure 4). LECs were stimulated in vitro with the indicated growth factors for the indicated times. Activation of ERKs and AKT was determined by Western blotting of cell lysates with phosphospecific antibodies. Blots were reprobed with ERK and AKT antibodies to demonstrate equivalent protein loading. Experiments were repeated at least 3 times with the same results. (**C**) Purified LECs were stimulated with medium alone or with medium containing the indicated growth factors for 48 hours. Proliferation was assessed by BrdU incorporation during the last 24 hours of culture and measured by BrdU ELISA kit. Results are mean + 1 SD of triplicate determinations. (**D**) Purified LECs were grown to confluency and then cultured in the presence or absence of serum with ECGS for a further 72 hours. Apoptosis was determined by annexin V staining and flow cytometry. Numbers denote percent annexin V$^+$ cells among total live 7-AAD$^-$ cells. Experiments in **C** and **D** were repeated 3 times with similar results.

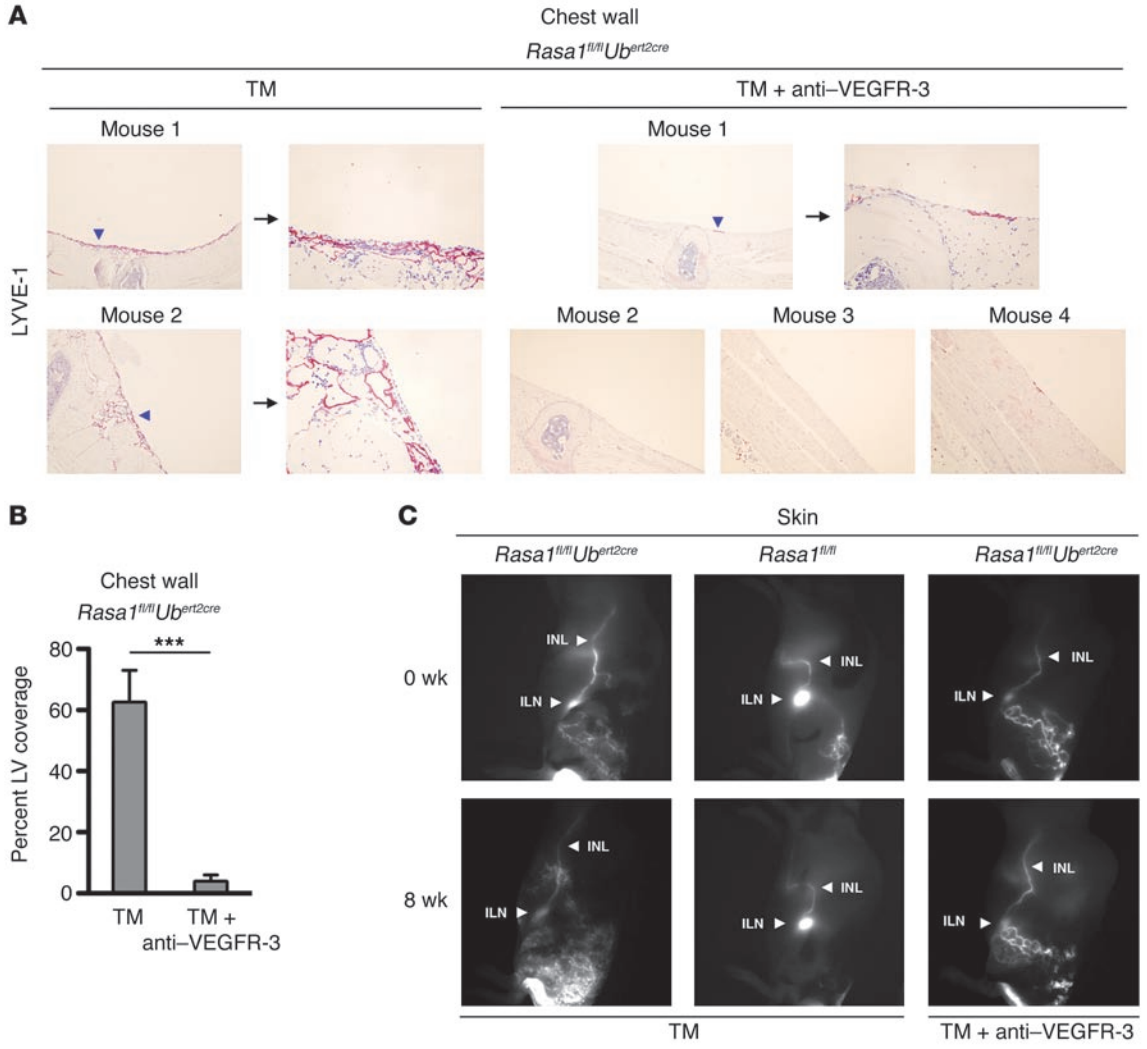

Figure 10

VEGFR-3 blockade inhibits the development of lymphatic vessel hyperplasia in induced RASA1-deficient mice. (**A**–**C**) *Rasa1*$^{fl/fl}$*Ub*^{ert2cre} and *Rasa1*$^{fl/fl}$ mice were injected at 2 months of age with TM alone or TM together with a blocking anti–VEGFR-3 antibody that was readministered to mice every 3 days for 8 weeks. (**A**) Chest walls were stained with an anti–LYVE-1 antibody (purple). Images from 2 TM-treated and 4 TM plus anti–VEGFR-3–treated mice are shown; arrows indicate enlarged views. Original magnification, ×40; ×100 (enlargements). (**B**) Percent lymphatic vessel coverage of the inner surface of the chest wall facing the pleural cavity. Data (mean + 1 SEM) are derived from measurements made on 12 longitudinal and cross-sections of thorax from 3 (TM) or 4 (TM plus anti–VEGFR-3) mice. ***$P < 0.001$. (**C**) NIR fluorescent images of dermal lymphatic vessels immediately prior to and 8 weeks after treatment. Images were acquired 15 minutes after ICG injection. See also Supplemental Videos 5 and 6. The same results were obtained with 3 other *Rasa1*$^{fl/fl}$*Ub*^{ert2cre} mice treated with anti-VEGFR-3 antibody ($n = 4$ total).

We also examined Ras-MAPK signal transduction in BECs and fibroblasts from induced RASA1-deficient adult mice (Supplemental Figure 5). For BECs, we examined signaling in response to PDGF, FGF, and VEGF-A; for fibroblasts, we examined signaling in response to PDGF and EGF. In BECs, PDGF-induced MAPK activation was increased upon loss of RASA1 at the peak of the response, although the kinetics of MAPK activation was not altered. In contrast, for FGF, MAPK activation occurred earlier in RASA1-deficient BECs, although no difference in the magnitude of the response was apparent. For VEGF-A, both the magnitude and kinetics of MAPK activation were the same between RASA1-deficient and control BECs. In RASA1-deficient fibroblasts, the magnitude of MAPK activation (or AKT activation) induced by PDGF and EGF was generally reduced compared with control fibroblasts, although the kinetics of responses was unaltered. These findings may contribute to an understanding of why TM-induced *Rasa1*$^{fl/fl}$*Ub*^{ert2cre} mice show a spontaneous phenotype only in the lymphatic vascular system (see Discussion).

Increased proliferation and survival of RASA1-deficient LECs in vitro. Since growth factor–induced Ras activation in RASA1-deficient LECs was dysregulated, we next assessed functional responses of purified LECs in vitro. No significant differences between RASA1-deficient and control LECs were noted in assays that measured LEC adhesion to substratum or LEC-LEC intercellular adhesion (measured by electrical resistance of monolayers), LEC migration (measured in wound healing and transwell migration assays), or tube formation on matrigel or collagen matrices either in the presence or absence of growth factors (data not shown). In contrast, as

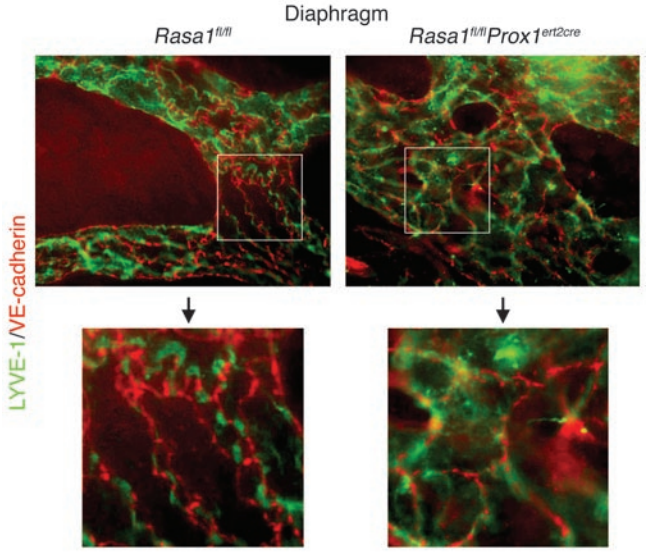

Figure 11
Junctional integrity of lymphatic vessels in induced RASA1-deficient mice. Whole mount diaphragm specimens from *Rasa1*$^{fl/fl}$*Prox1*^{ert2cre} mice with chylothorax and *Rasa1*$^{fl/fl}$ littermate controls were stained with LYVE-1 (green) and VE-cadherin (red) antibodies. Shown are initial lymphatic vessels in the central diaphragm; arrows indicate enlarged views of boxed regions. The same results were observed in *Rasa1*$^{fl/fl}$*Ub*^{ert2cre} mice with chylothorax (n = 4). Original magnification, ×400; ×1,000 (enlargements).

measured in BrdU incorporation assays in vitro, RASA1-deficient LECs proliferated more vigorously, as observed when LECs were stimulated with the combination of PDGF, FGF, and VEGF-C (Figure 9C). Individual growth factors were unable to stimulate proliferation of control or RASA1-deficient LECs in these assays (data not shown). In addition, RASA1-deficient LECs were less susceptible to apoptosis induced by serum and growth factor deprivation than were control LECs (Figure 9D).

Blockade of VEGFR-3 in vivo is sufficient to prevent lymphatic hyperplasia induced by loss of RASA1 in adult mice. Since the greatest differences in Ras signaling in RASA1-deficient LECs were observed after stimulation with VEGF-C (Figure 9B), we next sought evidence that dysregulated signal transduction through VEGFR-3 is required for the development of lymphatic vessel hyperplasia in vivo. At 2–3 months of age, *Rasa1*$^{fl/fl}$*Ub*^{ert2cre} mice were administered TM plus a blocking anti–VEGFR-3 antibody (mF4-31C1) that was readministered to mice every 3 days for 8 weeks (28). Lymphatic vessel hyperplasia in the chest wall was assessed by immunohistochemistry and in skin by NIR fluorescence imaging (Figure 10). Strikingly, anti–VEGFR-3 antibody treatment almost completely blocked the development of lymphatic hyperplasia in the chest wall (Figure 10, A and B). In contrast, littermate mice treated with TM alone or with TM plus an antibody of irrelevant specificity that was isotype-matched to the anti–VEGFR-3 antibody developed lymphatic hyperplasia at this site (Figure 10, A and B, and data not shown), as described above. In addition, anti–VEGFR-3 substantially blocked lymphatic hyperplasia in the skin of induced RASA1-deficient mice (Figure 10C and Supplemental Videos 5 and 6). We concluded that dysregulated Ras signal transduction initiated by VEGFR-3 on LECs is a major contributing factor to the development of spontaneous lymphatic vessel hyperplasia in induced RASA1-deficient mice.

Disruption of button-like tight junctions between LECs in initial lymphatics of induced RASA1-deficient mice with chylothorax. The relationship between lymphatic vessel hyperplasia and chylothorax and chylous ascites development in induced RASA1-deficient mice is uncertain. Potentially, massive lymphatic vessel overgrowth at affected sites could predispose vessels to mechanical damage and local rupture. Alternatively, loss of RASA1 expression may have a direct effect on LEC junctional integrity. Recent work has established the presence of specialized discontinuous button-like junctions between LECs in initial lymphatics that are composed of VE-cadherin and tight junction–associated proteins (22). These buttons border overlapping flaps between LECs and are essential for the maintenance of junctional integrity. Therefore, we closely examined the junctions between LECs in initial lymphatic vessels in induced RASA1-deficient mice that had developed chylothorax. Whole mount diaphragm specimens were double stained with anti–VE-cadherin and anti–LYVE-1 antibodies (Figure 11). In TM-treated control mice, we readily identified VE-cadherin–containing buttons positioned at the periphery of LECs between LYVE-1–rich flaps. Conversely, in TM-treated RASA1-deficient mice that had developed chylothorax, VE-cadherin buttons were rarely identified, and the expression patterns of VE-cadherin and LYVE-1 at LEC borders were mostly overlapping. These findings strongly support the notion that RASA1 is required for the maintenance of LEC junctional integrity, which explains, at least in part, the development of chylothorax and chylous ascites in induced RASA1-deficient mice.

Discussion

We show here that induced systemic deletion of *Rasa1* from adult mice resulted in a spontaneous disorder of the lymphatic vascular system. Loss of RASA1 caused extensive lymphatic vessel hyperplasia that was a consequence of dysregulated LEC proliferation. In addition, loss of RASA1 caused a lymphatic vessel leakage defect associated with the development of chylothorax, chylous ascites, and death. These findings identified RASA1 as a critical regulator of the lymphatic vessel growth and function required for the integrity of the lymphatic vasculature in resting animals.

To determine whether lymphatic vessel phenotypes in induced RASA1-deficient mice were LEC intrinsic, we used a *Prox1*^{ert2cre} knockin line, in which expression of Ert2Cre is driven by the endogenous *Prox1* promoter (21). Reporter analysis confirmed that Ert2Cre was active predominantly in lymphatic vessels in this line. A recent report showed that Prox1 is also expressed in venous valves and that in a *Prox1*^{ert2cre} BAC transgenic mouse line, Ert2Cre is active in venous valve endothelial cells as well as lymphatics (29). Conversely, we were unable to detect Cre-mediated recombination in the blood vascular system using the *Prox1*^{ert2cre} knockin line described herein. Potentially, this discrepancy could be explained by differences in the level of Ert2Cre expression between lines and/or differences in the TM administration protocol.

Loss of RASA1 specifically in LECs of adult mice was shown to be sufficient for the development of lymphatic vessel growth defects. Hyperplasia of lymphatic vessels in the skin and diaphragm was noted, although in the latter tissue, the extent of hyperplasia was less than that observed upon ubiquitous deletion of *Rasa1*. In contrast, chylothorax did not develop in adult LEC-specific RASA1-deficient mice. One interpretation of this finding is that development of chylothorax is LEC extrinsic. However, it is more likely that the absence of chylothorax can be explained by relatively weak activity of *Prox1*^{ert2cre} versus *Ub*^{ert2cre} in lymphatic vessels. In the *Prox1*^{ert2cre}

line, Cre-mediated recombination was detected in a minority of LECs in initial and collecting lymphatics, whereas in the *Ub*^{ert2cre} line, Cre activity was detected in all LECs. Thus, in order for chylothorax to manifest, a threshold level of *Rasa1* deletion may have to be surpassed. In support of this, *Rasa1*$^{fl/fl}$*Prox1*^{ert2cre} mice that had been induced with TM at E15 of development, which would be predicted to result in more efficient *Rasa1* deletion in LECs, did develop chylothorax 2 weeks after birth.

The LEC-intrinsic nature of the hyperplastic lymphatic vessel phenotype, together with the finding that MAPK was constitutively active in RASA1-deficient LECs in situ, suggested a model in which abnormal spontaneous lymphatic vessel growth arises as a result of dysregulated LEC growth factor receptor signal transduction to the low ligand concentrations normally present in resting tissues. According to this model, in wild-type mice, these ligands would continually initiate activation of Ras in LECs. However, owing to the action of RASA1, this activated Ras would be quickly converted back to the inactive GDP-bound form. In contrast, in RASA1-deficient mice, activated Ras molecules would accumulate, which in turn would result in dysregulated LEC proliferation and survival and overgrowth of the lymphatic vascular system.

Analysis of purified LECs in vitro revealed that Ras signal transduction initiated by PDGFR, FGFR, and VEGFR-3, but not by VEGFR-1 or VEGFR-2, was dysregulated in the absence of RASA1. Specifically, PDGF and FGF stimulated slightly prolonged activation of MAPK in RASA1-deficient LECs. Moreover, whereas VEGF-C stimulated a monophasic activation of MAPK and AKT in control LECs, a biphasic activation of both kinase types was observed in RASA1-deficient LECs. In parallel with these findings, RASA1-deficient LECs showed increased proliferation and survival in response to stimulation with the combination of all 3 growth factors in vitro. RASA1 has previously been implicated in the regulation of FGFR- and PDGFR-induced Ras activation (30, 31). To our knowledge, a similar role for RASA1 as a regulator of VEGFR-3–induced Ras activation has not been reported. However, like the other 2 receptors, VEGFR-3 contains cytoplasmic domain tyrosine residues in canonical motifs that would allow recognition by RASA1 SH2 domains and thus recruitment of RASA1 to membranes during the course of receptor signaling. It is likely that dysregulated Ras signal transduction through VEGFR-3 is the dominant factor that drives lymphatic hyperplasia in induced RASA1-deficient mice. This would be consistent with the finding that anti–VEGFR-3 blockade almost completely inhibited lymphatic vessel hyperplasia in the chest region of induced RASA1-deficient mice and had a significant inhibitory effect on lymphatic vessel hyperplasia in the skin.

Spontaneous blood vessel abnormalities were not observed in adult TM-induced *Rasa1*$^{fl/fl}$*Ub*^{ert2cre} mice. This cannot be explained by ineffective deletion of *Rasa1* in BECs, since in Cre reporter mice, the *Ub*^{ert2cre} transgene was shown to be highly active in blood vessels. Moreover, as shown by Western blotting, in *Rasa1*$^{fl/fl}$*Ub*^{ert2cre} mice, RASA1 expression in BECs was essentially extinguished in BECs (Supplemental Figure 5). One reason for the lack of a spontaneous blood vessel abnormality after loss of RASA1 in adult mice may be a redundancy of RASA1 with other RasGAPs in BECs. In this regard, extended activation of the Ras-MAPK pathway in response to different growth factors was not observed in RASA1-deficient BECs as it was in RASA1-deficient LECs. A second basis for the lack of a spontaneous blood vessel phenotype may be that activation of Ras by itself is not sufficient to drive BEC proliferation. This is indicated by the finding that transgenic overexpression of Ras in LECs and BECs in mice results in the same development of lymphatic vessel hyperplasia, but not blood vessel abnormalities, as described here (10).

Although a spontaneous blood vessel phenotype was not observed in adult induced RASA1-deficient mice, it is important to point out that RASA1 does play an important role in the blood vascular system in adults during pathological angiogenesis. Thus, microRNA-mediated loss of RASA1 is essential for blood vessel angiogenesis toward tumors (6). RASA1 is also critical for blood vessel function during development. In RASA1-deficient embryos, there is a failure of normal blood vessel patterning in both the yolk sac and the embryo itself, which leads to embryonic death (5). Furthermore, as shown here, this was consequent to loss of RASA1 specifically in BECs (Supplemental Figure 1). Whether blood vascular defects in RASA1-deficient embryos develop as a result of aberrant Ras activation in BECs is uncertain (32, 33). RASA1 has been shown to be required for directed cell movement, the impairment of which may instead underlie defective blood vessel patterning in RASA1-deficient embryos. Importantly, RASA1 is thought to regulate directed cell movement in a manner independent of its ability to regulate Ras, but rather dependent on physical interaction with p190 RhoGAP, which functions as a GAP for the Ras-related Rho small GTP-binding protein.

In humans with CM-AVM, mutations of the *RASA1* gene do cause spontaneous blood vascular lesions in children and adults (7–9). This could reflect a genuine species difference between humans and mice with regard to the role of RASA1 in regulation of the mature blood vasculature. However, in CM-AVM, RASA1 loss through second-hit mutation may occur during embryonic development. In contrast, in the induced RASA1-deficient mouse model described here, expression of RASA1 remained intact throughout embryonic development. Therefore, should loss of RASA1 during development be necessary for the appearance of spontaneous blood vascular abnormalities that present after birth, differences in the timing of RASA1 loss in CM-AVM and in the induced RASA1-deficient mouse model could account for the differences in phenotype.

Interestingly, chylothorax and chylous ascites have been observed in a small number of CM-AVM patients (9). Because chylothorax and chylous ascites are rare in humans, a spontaneous lymphatic vessel phenotype resulting from loss of RASA1 expression appears to be conserved across species. It is possible that a larger number of CM-AVM patients show lymphatic abnormalities, such as hyperplasia, that may be revealed by noninvasive NIR fluorescence imaging (34, 35). Alternatively, an apparent lower incidence of lymphatic abnormalities in CM-AVM could be explained by a requirement for second-hit mutations in LECs in order for lymphatic vessel lesions to manifest. Such second-hit mutations would be expected to occur in only a minority of LECs. This contrasts with the induced RASA1-deficient mouse, in which the vast majority of LECs would lose expression of RASA1.

VE-cadherin–rich button-like junctions between LECs in initial lymphatics of the chest region were disrupted in induced RASA1-deficient mice. This finding provides a potential explanation for lymphatic vessel leakage in this model. Notably, both tissue edema and chylothorax develop in mice that overexpress Ras in LECs (10). This suggests that the lymphatic vessel leakage defects that occur after RASA1 loss are consequent to aberrant Ras activation in LECs. However, how aberrant Ras activation relates to disruption of button-like junctions remains to be established.

Outside of the lymphatic vascular system, no significant abnormalities have been detected in any other tissue in induced RASA1-deficient mice. One exception is the immune system, where T cell development and survival is affected (36). However, T cell phenotypes in induced RASA1-deficient mice and T cell–specific constitutive RASA1-deficient mice are relatively subtle, and which RasGAPs regulate antigen-induced Ras activation in mature T cells remains to be defined. Likewise, despite its broad pattern of expression, RASA1 does not appear to be a significant nonredundant regulator of Ras activation in other somatic cell types (including fibroblasts; Supplemental Figure 5). In particular, induced RASA1-deficient mice did not develop tumors in any tissue; thus, RASA1 did not function as an essential tumor suppressor.

In summary, we showed here that RASA1 functions as a nonredundant physiological negative regulator of lymphatic vessel growth that is required for the maintenance of normal lymphatic vessel architecture and functional integrity in adult animals. These findings have important implications for our understanding of mechanisms of lymphatic vessel growth and function in general. In addition, prior findings suggest that RASA1 may be a useful target for the manipulation of lymphatic vessel growth in disease situations (37). For example, in lymphedema, local short-term inhibition of RASA1 expression could promote local lymphatic vessel growth, resulting in symptom alleviation. Conversely, in cancer, prevention of growth factor–mediated downregulation of RASA1 in LECs, which may be required for tumor-induced lymphangiogenesis, could result in reduced tumor metastasis. One possible way in which such manipulation could be achieved is through the use of RASA1-specific microRNAs and counterpart anti-microRNAs that have previously been described and shown to be effective in manipulation of blood vessel angiogenesis in vivo (6).

Methods

Mice. *Rasa1*$^{fl/fl}$ and *Ub*^{ert2cre} mice have been described previously (11, 38). *Prox1*^{ert2cre} mice were provided by G. Oliver (St. Jude Children's Hospital, Memphis, Tennessee, USA) (21). Mice carrying a *Tie1-Cre* transgene were purchased from the European Mutant Mouse Archive. Mice were intercrossed to generate *Rasa1*$^{fl/fl}$*Ub*^{ert2cre}, *Rasa1*$^{fl/fl}$*Prox1*^{ert2cre}, and *Rasa1*$^{fl/fl}$*Tie1-Cre* mice and littermate controls. Reporter *Rosa26*^{eyfp} mice, purchased from JAX (12), were crossed with *Ub*^{ert2cre} and *Prox1*^{ert2cre} mice to generate *Rosa26*^{eyfp}*Ub*^{ert2cre} and *Rosa26*^{eyfp}*Prox1*^{ert2cre} mice. All mice were on a mixed 129S6/SvEv X C57BL/6 genetic background.

TM administration. Adult mice at age 2 months and pregnant dams were given 2 i.p. injections of TM (0.2 mg/g body weight per injection, dissolved in corn oil; MP Biochemicals) on consecutive days. For antibody blocking experiments, an anti–VEGFR-3 monoclonal antibody (mF4-31C1, 0.8 mg antibody per mouse per injection; provided by B. Pytowski, ImClone Systems, New York, New York, USA) was administered i.p. to mice at the same time as TM and every 3 days thereafter for 8 weeks (28).

Triglyceride analysis. Levels of triglycerides in plural effusions were determined with the use of an IDEXX analyzer (IDEXX Laboratories) using dry chemistry.

Evans blue tracing. For thoracic duct drainage experiments, Evans blue (5 mg/ml in PBS; Sigma-Aldrich) was injected s.c. into hind foot pads and the base of the tail (50 μl at each injection site). After 1 hour, mice were euthanized, and drainage of dye to the thoracic duct was examined. For examination of dermal lymphatics, Evans blue was injected i.d. at the base of the tail of shaved mice (20 μl per injection). Dermal lymphatics were imaged 1 minute afterward. Subsequently, mice were euthanized, and a midline incision was made to expose lymphatics on the underside of the skin and the inguinal LN.

Tissue immunostaining. For preparation of tissue sections, mice were euthanized, and organs were fixed in 4% paraformaldehyde and embedded in paraffin. For chest wall, samples were decalcified before embedding. For whole mount staining, mice were perfused with 1% paraformaldehyde before organ explantation. 5-μm sections or whole organs were stained with rat or rabbit anti–LYVE-1 (Upstate Biotechnology, Abcam, and eBioscience); rabbit anti-Prox1 (Millipore) and anti-GFP (Abcam); mouse anti-SMA (Sigma-Aldrich) and anti–phospho-ERK (Cell Signaling Technology); and rat anti–VEGFR-3 (eBioscience), anti-CD31 (BD Biosciences), and anti–VE-cadherin (Abcam) primary antibodies. For immunofluorescence detection, secondary goat anti-rabbit Alexa Fluor 488, goat anti-mouse Alexa Fluor 594, or goat anti-rat Alexa Fluor 594 antibodies were used (Invitrogen). For immunohistochemistry, a rabbit on rodent AP Polymer kit (Biocare) was used. Either DAB or Vulcan Fast Red (Biocare) were used as chromagens. Sections were viewed on an Olympus IX70 microscope. Lymphatic vessel density and diameter was determined as described previously (39).

NIR fluorescence imaging. NIR fluorescence imaging was performed as described previously (19, 20). 20 μl ICG (555 μM) was injected i.d. at the base of the tail of shaved mice. Fluorescence images were acquired with 200-ms integration time by an electron-multiplying CCD camera (Princeton Instruments). Data were analyzed with Matlab (The Mathworks) and ImageJ (NIH). Pulsatile activity was determined by measuring the mean fluorescence intensity at selected ROIs with respect to time.

Cell isolation. For isolation of LECs and BECs, lungs were minced with scissors and digested with 0.25% collagenase D (Roche) for 1 hour at 37°C. Single cell suspensions were prepared by mechanical disruption followed by passage through a 70-μm cell strainer (BD Biosciences). Cell suspensions were incubated with an anti-podoplanin antibody (8F11; MBL), and LECs were isolated by positive selection using goat anti-rat–coated immunobeads (Miltenyi). BECs were similarly isolated from LEC-depleted lung cell suspensions using an anti-CD31 antibody (Abcam). LECs and BECs were seeded into collagen-coated wells of 24-well tissue culture plates and expanded by culture in DMEM supplemented with 20% fetal calf serum (complete medium), 100 μg/ml heparin, and 3 μg/ml ECGS (Sigma-Aldrich) for 5–7 days. For isolation of fibroblasts, 1-cm sections of tail were digested with 0.25% collagenase D (Roche) overnight. Released cells were then cultured in complete medium for 10 days.

Flow cytometry. Pleural effusion cells from deceased mice and peritoneal exudate cells (obtained by lavage) from euthanized mice were stained with fluorochrome-labeled TCRβ (H57-597), CD19 (1D3), B220 (RA36B2), CD11b (M1-70), Gr1 (RB6-8C5), CD4 (GK1.5), and CD8 (53-6.7) mAbs (all from BD Biosciences). Whole cell suspensions from lung and isolated LECs were stained with CD45.2 (104; BD Biosciences), podoplanin (8.1.1; BioLegend), CD31 (MEC 13.3; BD Biosciences), LYVE-1 (Abcam), VEGFR-3 (AF743; R&D Systems), α9 integrin (R&D Systems), and Ep-CAM (G8.8; BioLegend) antibodies. Antibodies were either directly fluorochrome-labeled or were detected with appropriate fluorochrome-labeled secondary antibodies. Cell staining was analyzed by flow cytometry on a FACSCanto (BD Biosciences).

LEC proliferation in vivo. 8 days after TM administration, mice were injected i.p. with 1 mg BrdU (Roche) by i.p. injection. The BrdU injection was repeated 2 days later. 2 hours after the second BrdU injection, diaphragms were harvested from mice and subjected to whole mount staining using rabbit anti–LYVE-1 and mouse anti-BrdU (Millipore) antibodies and corresponding secondary Alexa Fluor–conjugated secondary antibodies. Alternatively, mice were injected with BrdU 3 and 5 days after TM. 2 hours after the last BrdU injection, lungs were harvested from mice, and whole cell suspensions were prepared. Incorporation of BrdU into LECs and BECs was determined by flow cytometry as described above using a directly coupled anti-BrdU antibody (BD Biosciences).

Cell signal transduction. Cells were detached from plastic by incubation in Accutase (Sigma-Aldrich) and seeded in DMEM into wells of 96-well plates (5×10^4 cells/well) coated (LECs and BECs) or not (fibroblasts) with collagen. After overnight culture, cells were stimulated with 100 ng/ml murine PDGF-ββ (BioVision), murine FGF (R&D Systems), rat VEGF-C (Genway), or murine VEGF-A (R&D Systems) for different times at 37°C. Cells were then lysed in nonident P-40 lysis buffer, and activation of ERK and AKT was determined by Western blotting of cell lysates using phospho-specific anti-ERK and anti-AKT antibodies (Cell Signaling Technology). Blots were reprobed with anti-ERK, anti-AKT, and anti-GAPDH antibodies (Cell Signaling Technology) to confirm equivalent protein loading. Equivalent expression of PDGFR and FGFR-3 was shown by Western blotting of RASA1-deficient and control LEC lysates using specific antibodies (Abcam). Loss of RASA1 expression in RASA1-deficient LECs was also shown by Western blotting using a specific antibody (Santa Cruz Biotechnology).

LEC proliferation. Detached LECs were seeded in DMEM with 5% fetal calf serum into collagen-coated wells of 96-well plates (3×10^3 cells/well). The following day, cells were stimulated with growth factors as described above. After 24 hours, BrdU was added to the cultures, which were incubated for an additional 24 hours. Incorporation of BrdU was measured using a cell proliferation ELISA kit (Roche).

LEC survival. LECs were grown to confluency in wells of 24-well plates. Wells were then washed, and either DMEM or DMEM supplemented with 20% fetal calf serum, heparin, and ECGS was added back to wells. After 3 days, all cells in wells were harvested, and the extent of apoptotic cell death was assessed by staining with fluorochrome-coupled annexin V and 7-AAD (BD BioSciences). 7-AAD$^+$ cells were eliminated from analysis.

Statistics. Statistical analysis was performed using the Student's 2-sample *t* test. A *P* value less than 0.05 was considered significant.

Study approval. All experiments performed with mice were in compliance with University of Michigan and University of Texas Health Science Center–Houston guidelines and were approved by the respective university committees on the use and care of animals.

Acknowledgments

This work was supported by Public Heath Service grants RO1 HL096498 to P.D. King, AHA grant 11POST7580023 to P.E. Lapinski and P.D. King, and RO1 CA128919 to E.M. Sevick.

Received for publication December 15, 2010, and accepted in revised form November 30, 2011.

Address correspondence to: Philip D. King, Department of Microbiology and Immunology, University of Michigan Medical School, 6606 Med Sci II, 1150 West Medical Center Drive, Ann Arbor, Michigan 48109-5620, USA. Phone: 734.615.9073; Fax: 734.764.3562; E-mail: kingp@umich.edu.

1. Wennerberg K, Rossman KL, Der CJ. The Ras superfamily at a glance. *J Cell Sci*. 2005;118(pt 5):843–846.
2. Bos JL, Rehmann H, Wittinghofer A. GEFs and GAPs: critical elements in the control of small G proteins. *Cell*. 2007;129(5):865–877.
3. Chang L, Karin M. Mammalian MAP kinase signalling cascades. *Nature*. 2001;410(6824):37–40.
4. Bernards A. GAPs galore! A survey of putative Ras superfamily GTPase activating proteins in man and Drosophila. *Biochim Biophys Acta*. 2003; 1603(2):47–82.
5. Henkemeyer M, et al. Vascular system defects and neuronal apoptosis in mice lacking ras GTPase-activating protein. *Nature*. 1995;377(6551):695–701.
6. Anand S, et al. MicroRNA-132-mediated loss of p120RasGAP activates the endothelium to facilitate pathological angiogenesis. *Nat Med*. 2010; 16(8):909–914.
7. Boon LM, Mulliken JB, Vikkula M. RASA1: variable phenotype with capillary and arteriovenous malformations. *Curr Opin Genet Dev*. 2005; 15(3):265–269.
8. Eerola I, et al. Capillary malformation-arteriovenous malformation, a new clinical and genetic disorder caused by RASA1 mutations. *Am J Hum Genet*. 2003;73(6):1240–1249.
9. Revencu N, et al. Parkes Weber syndrome, vein of Galen aneurysmal malformation, and other fast-flow vascular anomalies are caused by RASA1 mutations. *Hum Mutat*. 2008;29(7):959–965.
10. Ichise T, Yoshida N, Ichise H. H-, N- and Kras cooperatively regulate lymphatic vessel growth by modulating VEGFR3 expression in lymphatic endothelial cells in mice. *Development*. 2010;137(6):1003–1013.
11. Lapinski PE, Bauler TJ, Brown EJ, Hughes ED, Saunders TL, King PD. Generation of mice with a conditional allele of the p120 Ras GTPase-activating protein. *Genesis*. 2007;45(12):762–767.
12. Srinivas S, et al. Cre reporter strains produced by targeted insertion of EYFP and ECFP into the ROSA26 locus. *BMC Dev Biol*. 2001;1:4.
13. Merrigan BA, Winter DC, O'Sullivan GC. Chylothorax. *Br J Surg*. 1997;84(1):15–20.
14. Ayadi A, et al. Net-targeted mutant mice develop a vascular phenotype and up-regulate egr-1. *EMBO J*. 2001;20(18):5139–5152.
15. Huang XZ, et al. Fatal bilateral chylothorax in mice lacking the integrin alpha9beta1. *Mol Cell Biol*. 2000; 20(14):5208–5215.
16. Makinen T, et al. PDZ interaction site in ephrinB2 is required for the remodeling of lymphatic vasculature. *Genes Dev*. 2005;19(3):397–410.
17. Harvey NL, et al. Lymphatic vascular defects promoted by Prox1 haploinsufficiency cause adult-onset obesity. *Nat Genet*. 2005;37(10):1072–1081.
18. Oliver G, Alitalo K. The lymphatic vasculature: recent progress and paradigms. *Annu Rev Cell Dev Biol*. 2005;21:457–483.
19. Kwon S, Sevick-Muraca EM. Noninvasive quantitative imaging of lymph function in mice. *Lymphat Res Biol*. 2007;5(4):219–231.
20. Kwon S, Sevick-Muraca EM. Functional lymphatic imaging in tumor-bearing mice. *J Immunol Methods*. 2010;360(1–2):167–172.
21. Srinivasan RS, et al. Lineage tracing demonstrates the venous origin of the mammalian lymphatic vasculature. *Genes Dev*. 2007;21(19):2422–2432.
22. Baluk P, et al. Functionally specialized junctions between endothelial cells of lymphatic vessels. *J Exp Med*. 2007;204(10):2349–2362.
23. Wigle JT, et al. An essential role for Prox1 in the induction of the lymphatic endothelial cell phenotype. *EMBO J*. 2002;21(7):1505–1513.
24. Wigle JT, Oliver G. Prox1 function is required for the development of the murine lymphatic system. *Cell*. 1999;98(6):769–778.
25. Garmy-Susini B, Makale M, Fuster M, Varner JA. Methods to study lymphatic vessel integrins. *Methods Enzymol*. 2007;426:415–438.
26. Shin JW, et al. Prox1 promotes lineage-specific expression of fibroblast growth factor (FGF) receptor-3 in lymphatic endothelium: a role for FGF signaling in lymphangiogenesis. *Mol Biol Cell*. 2006; 17(2):576–584.
27. Castellano E, Downward J. Role of RAS in the Regulation of PI 3-Kinase. *Curr Top Microbiol Immunol*. 2010; 346:143–169.
28. Pytowski B, et al. Complete and specific inhibition of adult lymphatic regeneration by a novel VEGFR-3 neutralizing antibody. *J Natl Cancer Inst*. 2005;97(1):14–21.
29. Bazigou E, et al. Genes regulating lymphangiogenesis control venous valve formation and maintenance in mice. *J Clin Invest*. 2011;121(8):2984–2992.
30. van der Geer P, Henkemeyer M, Jacks T, Pawson T. Aberrant Ras regulation and reduced p190 tyrosine phosphorylation in cells lacking p120-Gap. *Mol Cell Biol*. 1997;17(4):1840–1847.
31. Woodcock SA, Hughes DA. p120 Ras GTPase-activating protein associates with fibroblast growth factor receptors in Drosophila. *Biochem J*. 2004;380(pt 3):767–774.
32. Kulkarni SV, Gish G, van der Geer P, Henkemeyer M, Pawson T. Role of p120 Ras-GAP in directed cell movement. *J Cell Biol*. 2000;149(2):457–470.
33. Hu KQ, Settleman J. Tandem SH2 binding sites mediate the RasGAP-RhoGAP interaction: a conformational mechanism for SH3 domain regulation. *EMBO J*. 1997;16(3):473–483.
34. Sevick-Muraca EM, et al. Imaging of lymph flow in breast cancer patients after microdose administration of a near-infrared fluorophore: feasibility study. *Radiology*. 2008;246(3):734–741.
35. Rasmussen JC, Tan IC, Marshall MV, Fife CE, Sevick-Muraca EM. Lymphatic imaging in humans with near-infrared fluorescence. *Curr Opin Biotechnol*. 2009;20(1):74–82.
36. Lapinski PE, Qiao Y, Chang CH, King PD. A role for p120 RasGAP in thymocyte positive selection and survival of naive T cells. *J Immunol*. 2011; 187(1):151–163.
37. Karpanen T, Alitalo K. Molecular biology and pathology of lymphangiogenesis. *Annu Rev Pathol*. 2008;3:367–397.
38. Ruzankina Y, et al. Deletion of the developmentally essential gene ATR in adult mice leads to age-related phenotypes and stem cell loss. *Cell Stem Cell*. 2007;1(1):113–126.
39. Zhou F, et al. Akt/Protein kinase B is required for lymphatic network formation, remodeling, and valve development. *Am J Pathol*. 2010; 177(4):2124–2133.